

Article

Removal of Paracetamol from Aqueous Solutions by Photocatalytic Ozonation over $\text{TiO}_2\text{-Me}_x\text{O}_y$ Thin Films

Sorin Marius Avramescu^{1,2}, Irina Fierascu^{3,4,*}, Radu Claudiu Fierascu^{3,5,*}, Roxana Ioana Brazdis^{3,5}, Angel Vasile Nica², Claudia Butean⁶, Elena Alina Olaru², Sorin Ulinici⁷, Marian Nicolae Verziu⁸, and Anca Dumitru^{9,*}

- ¹ Department of Organic Chemistry, Biochemistry and Catalysis, Faculty of Chemistry, University of Bucharest, 050663 Bucharest, Romania; sorin.avramescu@g.unibuc.ro
- ² PROTMED Research Centre, University of Bucharest, 050107 Bucharest, Romania; nica.angelvasile@yahoo.ro (A.V.N.); alina.olaru@g.unibuc.ro (E.A.O.)
- ³ Emerging Nanotechnologies Group, National Institute for Research & Development in Chemistry and Petrochemistry—ICECHIM, 060021 Bucharest, Romania; roxana.brazdis@icechim.ro
- ⁴ Faculty of Horticulture, University of Agronomic Sciences and Veterinary Medicine of Bucharest, 011464 Bucharest, Romania
- ⁵ Department of Science and Engineering of Oxide Materials and Nanomaterials, Faculty of Chemical Engineering and Biotechnologies, University Politehnica of Bucharest, 011061 Bucharest, Romania
- ⁶ Department of Chemistry and Biology, North University Centre of Baia Mare, Technical University of Cluj-Napoca, 430122 Baia Mare, Romania; dee1168@yahoo.com
- ⁷ S.C. ICPE Bistrita S.A, 420035 Bistrita, Romania; sorin_ulinici@icpebn.ro
- ⁸ Department of Bioresources and Polymer Science, Advanced Polymer Materials Group, Faculty of Chemical Engineering and Biotechnologies, University Politehnica of Bucharest, 1-7 Gh Polizu Street, 011061 Bucharest, Romania; marian.verziu@upb.ro
- ⁹ Faculty of Physics, University of Bucharest, 077125 Magurele, Romania
- * Correspondence: irina.fierascu@icechim.ro (I.F.); fierascu.radu@icechim.ro (R.C.F.); anca.dumitru@gmail.com (A.D.)



Citation: Avramescu, S.M.; Fierascu, I.; Fierascu, R.C.; Brazdis, R.I.; Nica, A.V.; Butean, C.; Olaru, E.A.; Ulinici, S.; Verziu, M.N.; Dumitru, A. Removal of Paracetamol from Aqueous Solutions by Photocatalytic Ozonation over $\text{TiO}_2\text{-Me}_x\text{O}_y$ Thin Films. *Nanomaterials* **2022**, *12*, 613. <https://doi.org/10.3390/nano12040613>

Academic Editor: Baizeng Fang

Received: 31 December 2021

Accepted: 6 February 2022

Published: 11 February 2022

Publisher's Note: MDPI stays neutral with regard to jurisdictional claims in published maps and institutional affiliations.



Copyright: © 2022 by the authors. Licensee MDPI, Basel, Switzerland. This article is an open access article distributed under the terms and conditions of the Creative Commons Attribution (CC BY) license (<https://creativecommons.org/licenses/by/4.0/>).

Abstract: Analgesics and nonsteroidal anti-inflammatory drugs (NSAIDs) such as paracetamol, diclofenac, and ibuprofen are frequently encountered in surface and ground water, thereby posing a significant risk to aquatic ecosystems. Our study reports the catalytic performances of nanosystems $\text{TiO}_2\text{-Me}_x\text{O}_y$ (Me = Ce, Sn) prepared by the sol-gel method and deposited onto glass slides by a dip-coating approach in the removal of paracetamol from aqueous solutions by catalytic ozonation. The effect of catalyst type and operation parameters on oxidation efficiency was assessed. In addition to improving this process, the present work simplifies it by avoiding the difficult step of catalyst separation. It was found that the thin films were capable of removing all pollutants from target compounds to the oxidation products.

Keywords: catalytic ozonation; water treatment; paracetamol; photo-catalysis; thin films; titanium dioxide

1. Introduction

Water supplies are under a constant threat due to pollution resulting from numerous and complex anthropic activities. A special situation is represented by pharmaceuticals which escape traditional water treatment methods and reach the water bodies from multiple and almost uncontrollable sources [1–4]: effluents from pharmaceutical industries and hospitals, household disposal, the excretion of non-metabolized/metabolized drugs after human/animal consumption, aquaculture, sludge from water treatment facilities used as fertilizer and leaching drugs in ground water, etc. Moreover, along with parent compounds, the metabolites can also be harmful to aquatic ecosystems. The fraction of medicines that remain unchanged and leave patients' bodies ranges between 25% and 75% and, considering the large number of pharmaceuticals used worldwide, this results in a significant environmental burden which is growing due to an increase in world population

in number and age. Thus, in 2020, 4.5 trillion doses of different drugs were used and 50% of the world's population consume more than one dose [5] and, consequently, the concentration of pharmaceuticals in numerous natural water sources increase dramatically [6]. These compounds are encompassed (along with other largely used chemical compounds, such as hormones, plasticizers, wood treatment, pesticides, etc.) in the category of emerging pollutants (Eps) which are contaminants that are not currently regulated by environmental agencies. Another aspect of concern is that most of these compounds are also circumvented to the endocrine disruptor category that increases the danger for aquatic ecosystems.

Analgesics and nonsteroidal anti-inflammatory drugs (NSAIDs) like paracetamol, diclofenac, and ibuprofen are the most frequently encountered in surface and ground water, and therefore represent a significant risk for aquatic ecosystems [7,8]. Among them, paracetamol has an over-the-counter regime and is used intensively for pain relief and fever reduction. It is produced in staggering amounts, and the global acetaminophen market was valued at around US 850.5 million in 2020 and is expected to reach US 977.5 million in 2027, with a compound annual growth rate (CAGR) of around 2% [9]. In some countries, paracetamol consumption exceeds 20 g/person every year [10], thus it ends up in surface waters at concentrations of around 100 µg/L and surpasses tenfold the predicted non-effect concentration parameter (PNEC) which is 9.2 µg/L. Hence, considering the huge environmental impact of this compound and its metabolites, it is important to reduce the spreading of this drug in different aquatic ecosystems. In fact, it is primarily a containment problem and, as to solve this issue, paracetamol leaking must be stopped, preferably at the source. In order to fulfill this difficult task, it is necessary to use a versatile and efficient water treatment method, with large applicability in terms of aqueous effluents flow rate, source type, and the removal of target pollutants at the level requested by environmental regulation (which are subject to change toward lower values in a rapid pace). Catalytic ozonation is a technique with a significant capacity to accomplish these requirements in every respect due to the capability to oxidize/mineralize almost every organic pollutant [11–21]. Moreover, this method is a prominent example of advanced oxidation processes—a well-known category of water treatment approaches centered on using OH• radicals. This is the reason for a large number of studies regarding the development of catalytic systems capable of assisting the oxidative power of ozone mainly through the radical route. A large number of solids based on transitional metals in complex form or oxides, carbonaceous materials, etc., were studied for an evaluation of catalytic activity [22–30]. Additionally, catalyst precursors can be obtained from different industrial or agricultural wastes or pure metals salts. Despite that the catalytic ozonation process relies on a complex heterogeneous system (solid-gas-liquid), its performances are remarkable since most of these systems eliminate recalcitrant pollutants and set the quality parameters of treated water in the range established by environmental agencies. To be able to avoid the cumbersome separation step of the catalyst from treated water, a catalyst with a magnetic core was introduced [23,31–36]. Another interesting approach, that is unexploited in catalytic ozonation, although widely used in various other applications, is represented by thin films [37–44].

Well-known for its catalytic properties and chemical stability, TiO₂ represents a very good candidate for the development of new nanosystems with an environmental application, however, its photocatalytic applications are limited, as a consequence of the large band gap (~3.2 eV) and fast recombination of the exciton of TiO₂. This drawback can be overcome by the use of heterostructures of TiO₂ and metal oxides with lower valence bands (i.e., SnO₂), which hinders charge recombination, thus obtaining efficient photo-catalysis [45]. In an attempt to overcome another drawback in applying photo-catalysis to the treatment of polluted water (the recovery of the powder catalyst), TiO₂-based thin films, immobilized on different supports (aerogels, polymers, glass, etc.) were successfully proposed in the literature [46,47].

In this study, we report for the first time the removal of paracetamol from aqueous solutions using thin film catalysts based on TiO₂-Me_xO_y nanosystems deposited on glass plates

and immersed into a semi-batch reactor. The influence of catalyst type and operational parameters in oxidation efficiency was assessed.

2. Materials and Methods

2.1. Chemicals and Materials

Commercially available reagents with a purity higher than 98% for solid compounds and an HPLC grade for solvents were purchased from Sigma–Aldrich (Baden–Württemberg, Germany): paracetamol, Triton X-100 (X100, polyethylene glycol tert-octyl phenyl ether), titanium tetraisopropoxide (TTIP), tin (IV) chloride pentahydrate, cerium (III) nitrate hexahydrate, acetic acid (AcOH), ethanol (EtOH), acetonitrile (MeCN) and trifluoroacetic acid (TFA). Borosilicate glass slides (25 × 75 mm and a thickness of 1.0–1.2 mm) were obtained from Labbox (Barcelona, Spain). Airflow for ozone generation was provided by a laboratory compressor and distilled water with a resistivity of 18.2 MΩ.cm was used in all experiments.

2.2. Sol-Gel Synthesis

In sol-gel synthesis usually, a pore directing agent is used and Triton X100 (a nonionic surfactant with long chain) was selected for this study. Triton X100 is an inexpensive and nontoxic amphiphilic molecule, with a significant capacity to accommodate inorganic structures in aqueous liquids. A solution of ethanol, Triton X100, and acetic acid were prepared and, in this mixture, TTIP was introduced under vigorous stirring. The molar ratio of these components (X100:EtOH:AcOH:TTIP = 1:70:5:1) was selected in order to achieve a higher specific surface based on optimization studies undertaken by Stathatos et al. [48]. Acetic acid and ethanol release water upon esterification and consequently, slow hydrolysis of TTIP take effect. Additionally, the acetic acid replaces, to some extent, the alkoxy groups in TTIP. Each mentioned metals salt was added to separate flasks containing the above-prepared solution in quantities, so Me is 5% of the TTIP content except for two metal modified thin films, where the percent of metal attain a cumulative 10%.

2.3. Preparation of Thin Films

Glass slides were cleaned thoroughly in a succession of wash stages: detergent, water, acetone, and drying in N₂ flow. Thin films were deposited on slides using the dip-coating method using a programmable system (80C—PTL-SC-6-LD, MTI, New York, NY, USA) following several steps: immersion and extraction of slides from solution at a rate of 10 cm/min for three times with a 30 min pause between the dipping operation for drying at 60 °C. Finally, each slide was calcined in a multistep programmable furnace (Nabertherm L5/11, Neuhausen, Germany) at a ramp rate of 5 °C/min to 550 °C, maintained at 550 °C for 90 min and cooled down naturally. Prepared films on glass slides will be referred to as (Ti-Me) or (Ti-Me1-Me2) where Me = Ce, Sn.

2.4. Thin Films Characterization

The thin films' characterization was realized through several methods. The XRD patterns were recorded using Bruker D8 Discover equipment (Bruker AXS, Karlsruhe, Germany) (Cu_{kα1}, λ = 1.5406 Å), between 15 and 70° (2θ), in a grazing incidence configuration. The topography of the coated thin films was analyzed using an A.P.E Research SPM atomic force microscope (A.P.E. Research SRL, Trieste, Italy). DRIFT spectra of samples were collected in the region of 4000–500 cm⁻¹ at a resolution of 2 cm⁻¹ on a Varian 3100 Excalibur spectrometer (Walnut Creek, CA, USA) equipped with a Harrick Praying Mantis (Harrick Scientific Products, Inc., Pleasantville, NY, USA) diffuse reflectance accessory. UV–Vis absorption spectra of the films were carried out with a Helios alpha (Unicam, Cambridge, UK) spectrometer. The optical band gap [49–51] was evaluated by using the Tauc and Davis–Mott relation:

$$\alpha hv = A(hv - E_g)^n \quad (1)$$

where α is the absorption coefficient, A is an energy-independent constant, $h\nu$ stands for photon energy, E_g is the optical energy band gap, and n is considered to be the transition fingerprint. For $n = 1/2, 3/2, 2,$ and 3 , it can be distinguish direct allowed, direct forbidden, indirect allowed, and indirect forbidden transitions, respectively. Tauc graphs were developed by plotting $\alpha h\nu^n$ as a function of energy ($h\nu$), and the point where the tangent of the reverse-extension curve intersects with the x -axis represents the band gap value of a semiconductor [49].

Raman spectra were carried out using a Renishaw in Via Confocal Raman (Renishaw, Wotton-under-Edge, Gloucestershire, UK) microscope system. The excitation laser wavelength was 473 nm. The Raman spectra were acquired in the extended spectral region from 100 to 3200 cm^{-1} , under ambient conditions.

2.5. Photoreactor, Photocatalytic Activity, and Aqueous Effluents Analysis

All experiments regarding oxidation of paracetamol were performed in a semi-batch jacketed cylindrical reactor with a capacity of 250 mL equipped with a Pen-Ray UV Light Source 254 nm (Cole-Parmer, Vernon Hills, IL, USA) protected by a quartz tube and placed centrally (Figure 1). Ozone was obtained from dried air using an ozone generator (COM-AD-01, Anseros, Tübingen, Germany) and gas-phase ozone concentration was determined with an ozone analyzer (BMT 964, Stahnsdorf, Germany). The gas flow was supplied through a gas inlet into the reaction solution while simultaneously stirring at 1000 rpm, the temperature was kept at 20 °C using a thermostat, and solution pH was measured (PHM 240, Radiometer S.A.S., Neuilly-Plaisance, France) by an electrode inserted directly into the solution and maintained at 7 by adding HCl or NaOH trough liquid inlets. Samples were withdrawn at certain time intervals (5 to 30 min) to assure complete monitoring of the reaction course. The whole system was covered with aluminum foil as a deflector. Two or four glass slides with catalyst deposited on them were accommodated inside the reactor during the reaction. The reactor was filled with a 200 mL aqueous solution of paracetamol (100 mg/L). For repeated use, the catalytic slides were washed with distilled water and dried at 100 °C without any other treatment.

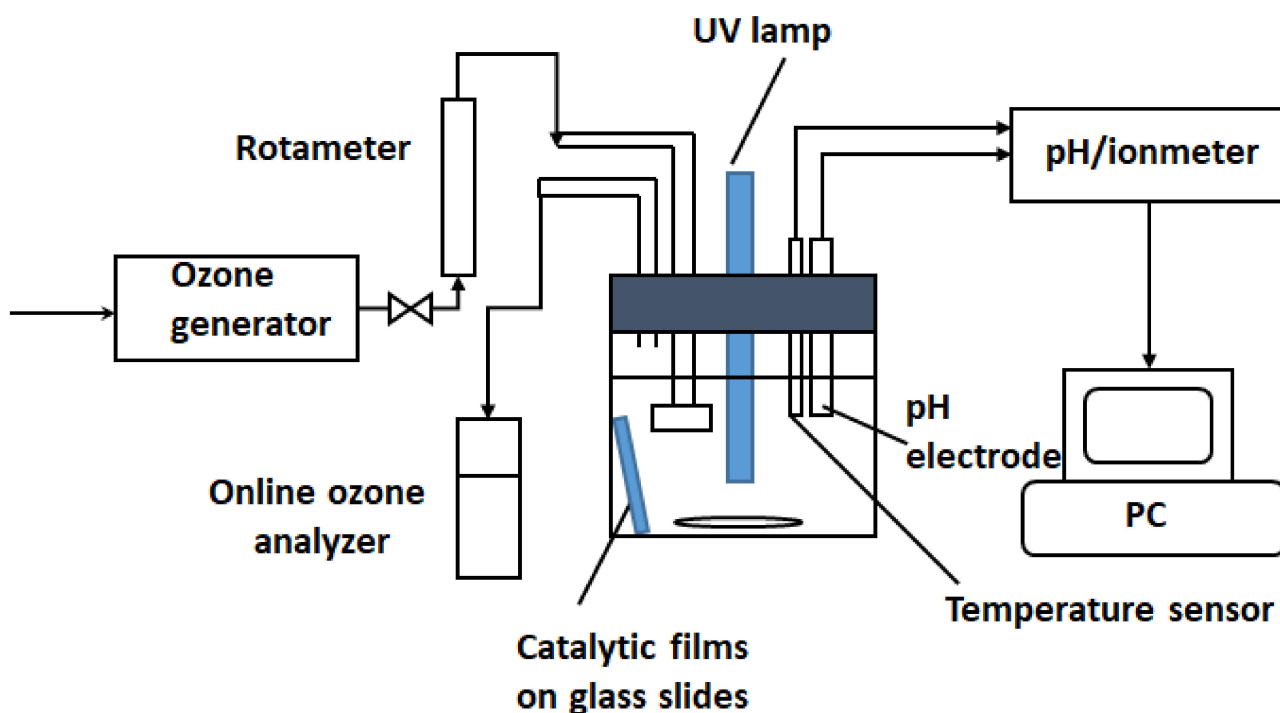


Figure 1. Experimental set-up for photocatalytic ozonation processes.

Paracetamol concentration was determined by the HPLC method using an L-3000 system (Rigol Technologies Inc., Beijing, China) consisting of a quaternary pump, a diode-array detector, and a Kinetex C18 Evo (150 mm × 4.6 mm i.d.; 5 μm particle size; Phenomenex, Torrance, CA, USA). Operating conditions were: isocratic elution of the mobile phase composed of eluent A (0.1% TFA in acetonitrile); eluent B (0.1% TFA in water) = 20:80, flow rate 1.0 mL/min, injection volume 10 μL, detection at 220 nm and 30 °C. Ammonia and nitrate ions were determined using a Varian HPLC system ProStar (Varian Analytical Instruments, Palo Alto, CA, USA) equipped with a conductometric detector, a conductivity suppressor, and Dionex cation or anion columns (IONPAC AS 19—4 × 250 mm or IonPac CS19—4 × 250 mm, Thermo Scientific, Waltham, MA, USA). Analysis was performed in isocratic mode with buffer carbonate/bicarbonate for nitrate and methanesulphonic acid for ammonia. Total organic carbon (TOC) measurements were achieved by the high-temperature oxidation method using a HiPerTOC (Thermo Electron, Waltham, MA, USA) analyzer. The absorbance of water samples at 254 nm (UV254) was measured using a Helios alpha (Unicam, Cambridge, UK) spectrometer.

3. Results and Discussions

3.1. Thin Film Characterization

The XRD patterns of the obtained materials are shown in Figure 2. The diffractograms of the as-prepared TiO₂ film reveal a typical anatase structure (according to pdf file 00-064-0863 from the International Centre of Diffraction Data 2019), with the most intense (101) peak at $2\theta = 25.08^\circ$ [52,53] and crystallite size of approximately 11.5 nm, calculated using the Debye–Scherrer equation using the (101) peak. The diffractograms also presents other peaks, corresponding to the diffraction planes (004), (112), (200), (105), (211), and (204) at $2\theta = 37.7, 38.6, 48.1, 53.9, 55.1$, respectively, 62.7° . The XRD pattern for as-prepared (Ti-Ce) shows an additional peak compared with TiO₂ films at around 30.3° , which is attributed to the Ce₂O₃ (101) plane according to pdf file 00-023-1048 from the International Centre of Diffraction Data 2019 [54]. According to literature data, the most probable explanation is related, on one hand, to a poor crystallization of the cerium oxide phase, which would not allow the indexation of other peaks, and on the other hand, to the low concentration of the phase, compared with the TiO₂ support [55–57]. Other authors [57] identified the presence of both CeO₂ and Ce₂O₃ phases in the XRD data; however, in our obtained diffractograms, no discernable peaks that can be attributed to a CeO₂ phase could be identified. The crystallite size of the TiO₂ phase was calculated to be approximately 12 nm, while the crystallite size of the the Ce₂O₃ phase was approximately 19 nm. The main conclusion is that Ce₂O₃ has little effect on the crystal structure of TiO₂. The XRD pattern of (Ti-Sn) films shows that the diffraction peaks corresponding to the anatase phase are slightly wider, with a crystallite size of approximately 13 nm. Additionally, the diffractogram reveals the presence of the specific amorphous phase peak, around 25° (2θ). Moreover, an additional contribution in the diffraction pattern of (Ti-Sn) films which are attributed to the tetragonal SnO₂ plane (110) can be observed at $2\theta = 26.6^\circ$, in concordance with pdf file data from the International Centre of Diffraction Data 2019 (00-005-0467), with a crystallite size corresponding to the SnO₂ phase over 20 nm. Several other minor peaks are present in the Ti-Sn diffractogram, which can be attributed to the presence of secondary phase, most probably Sn₂O₃ (ICDD PDF card no. 00-025-1259), as suggested by the presence of minor diffraction peaks at $2\theta = 27.4, 31.4, \text{ and } 55.9^\circ$, corresponding to the diffraction planes (011), (021), respectively (141). The diffraction pattern of as-prepared Ti-Ce-Sn does not show any diffraction peaks except an overlap contribution of around 25° (2θ), which indicates an amorphous nature of the thin film. Similar amorphous films were also reported by other authors, at a relatively Ti/Me ratio [58].

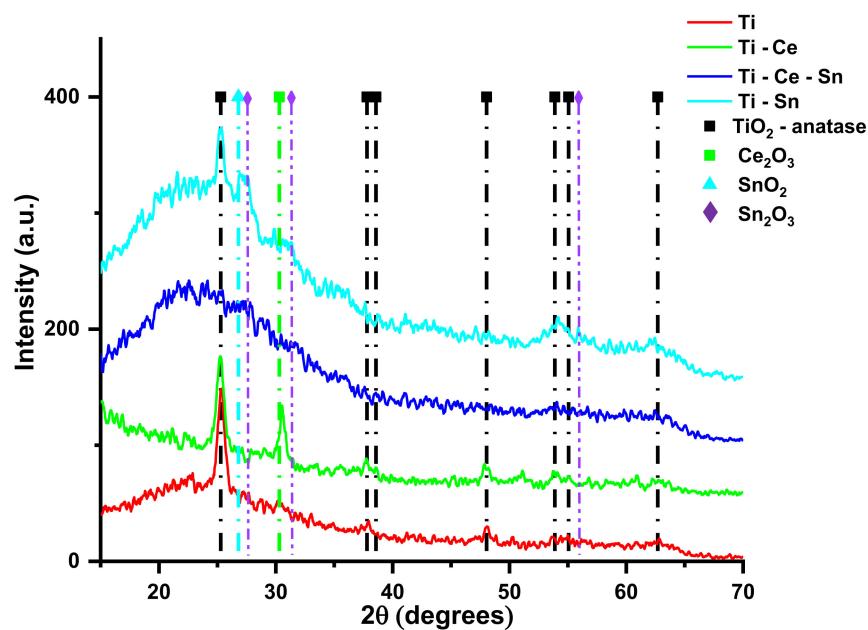


Figure 2. XRD patterns of $\text{TiO}_2\text{-Me}_x\text{O}_y$ films.

For the prepared thin films, AFM images and surface data are presented in Figure 3 and Table 1, showing that all modified $\text{TiO}_2\text{-Me}$ films were rougher than the simple TiO_2 films. In terms of catalytic activity, increased surface irregularities are subject to providing more active sites therefore faster removal of pollutants.

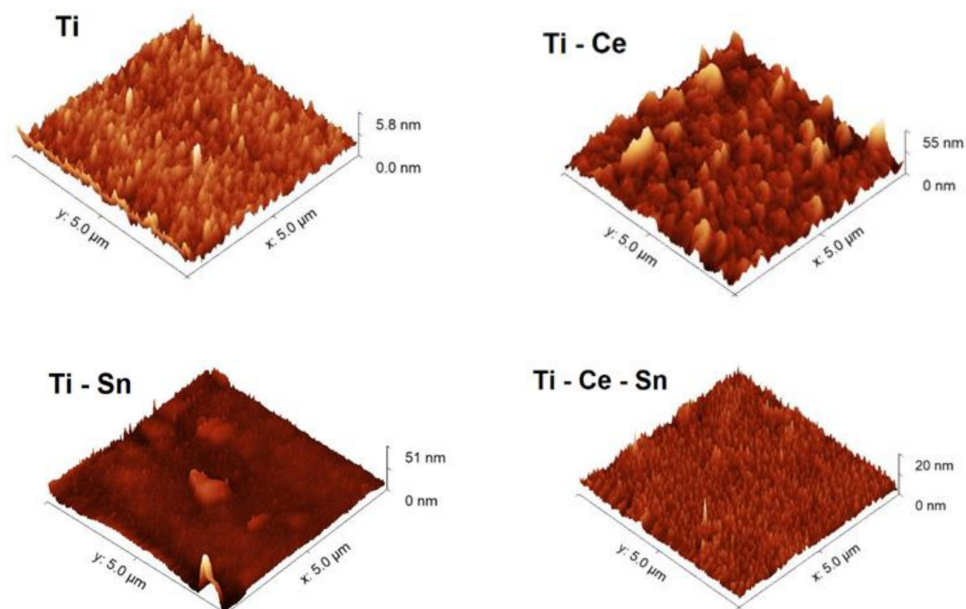


Figure 3. AFM images of $\text{TiO}_2\text{-Me}_x\text{O}_y$ films.

Table 1. The roughness of the prepared films.

Sample	RMS Roughness (nm)
(Ti)	1.1
(Ti-Ce)	5.9
(Ti-Sn)	2.97
(Ti-Ce-Sn)	2.1

Raman spectroscopy is a widely used tool to detect chemical bonds as well as to identify the crystalline state of metal oxides. Raman spectra (Figure 4) for all prepared films were performed under ambient conditions. The band at 143 cm^{-1} assigned to TiO_2 anatase structure [59] is well highlighted for all materials, except for the Ti-Ce-Sn sample, where the presence both of cerium and tin led to an increase of bands intensity at 244, 455, and 612 cm^{-1} which corresponds to the rutile phase [60]. Moreover, SnO_2 promotes the crystallization of the TiO_2 in the rutile phase [61,62], which justifies the presence of the bands' characteristics for rutile structure regarding the Ti-Sn films. On the other hand, in the presence of Ce, the Raman bands are below 700 cm^{-1} and could be assigned to TiO_2 as anatase [63].

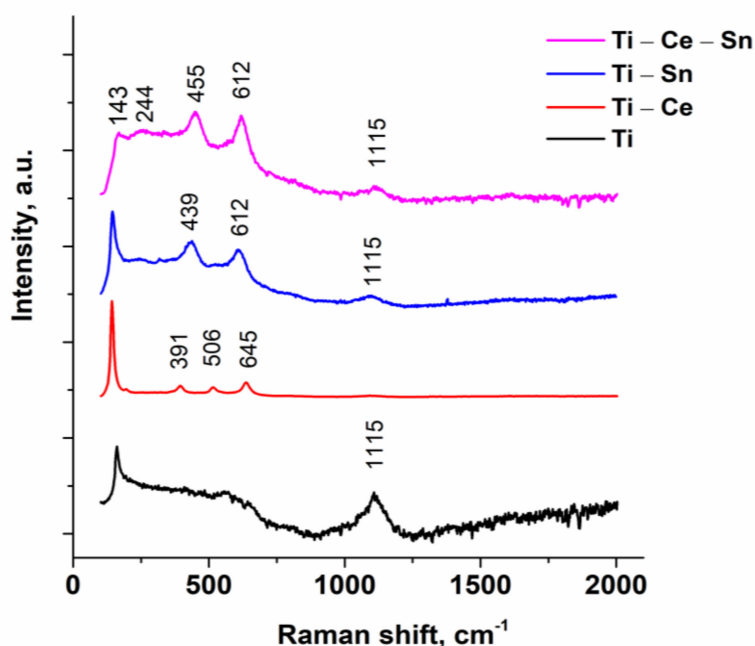


Figure 4. Raman spectra of prepared film.

Anatase presence is consistent with data obtained from XRD patterns. In the case of the (Ti-Ce) system, three bands at 391 , 506 and 645 cm^{-1} confirm the formation of crystalline CeO_2 [64,65]. The spectra for (Ti-Sn) systems present bands at 442 cm^{-1} with a shift at 455 cm^{-1} for (Ti-Ce-Sn), a result of E_g vibration mode for the rutile phase of SnO_2 and at 612 cm^{-1} for both systems attributed surface phonon modes of SnO_2 [66]. For all spectra, the band at 1115 cm^{-1} corresponds to a glass substrate.

FTIR spectra (Figure S1, Supplementary Material) were collected for pristine films and those used in the oxidation reaction. Borosilicate glass slides present a characteristic band assigned to Si-O bonds (559 , 1287 cm^{-1}), Bi-O (826 , 2162 cm^{-1}), OH groups (3532 cm^{-1}), and the spectra for (Ti) and (Ti-Ce) films mimics glass spectra, probably due to higher transparency. In the case of (T-Sn) and (Ti-Ce-Sn) systems, FTIR spectra are significantly flattened as the thickness increases. FTIR spectra were also used as a tool for assessing the preservation of film integrity during the oxidation process and it can be observed that the thin films preserve their integrity.

The UV-VIS absorption spectra and Tauc plots of modified TiO_2 thin films were presented in Figure 5 and the estimated band gaps (E_g) are presented in Table 2. Lower values of E_g for Ce modified films can be attributed to partial substitution of Ti cations and/or TiO_2 crystal size [67]. From the transmittance spectra, it can be observed that prepared films are highly transparent in the visible region with a red shift of (Ti-Ce), (Ti-Ce-Sn) compared with (Ti) and (Ti-Sn) and this is an indication that these films have a narrow bandwidth [65]. Increased transmission is also linked with film crystallinity [68] and consequently, to photocatalytic activity.

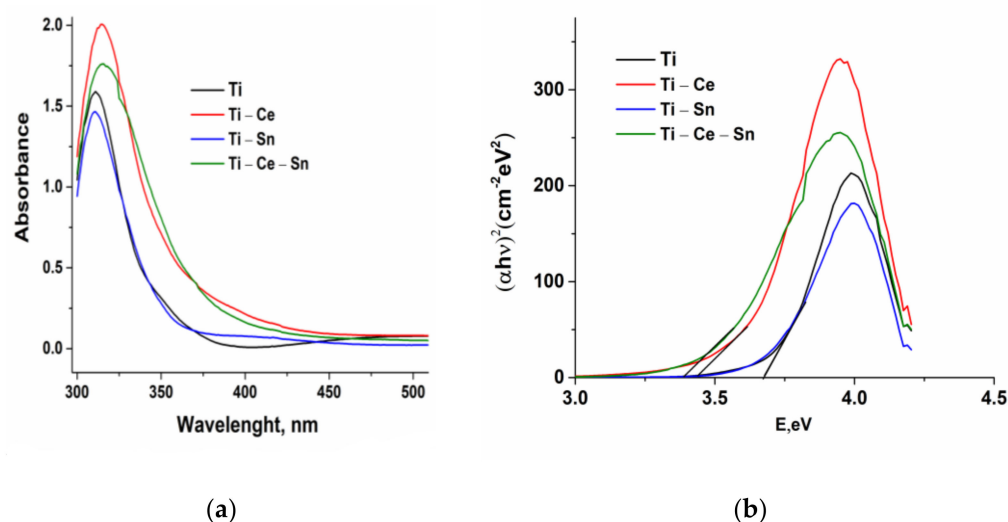


Figure 5. Absorbance data (a) and Tauc plot (b) for prepared films.

Table 2. Band gaps determined from UV-Vis spectra.

Sample	Band Gap
(Ti)	3.68
(Ti-Ce)	3.44
(Ti-Sn)	3.68
(Ti-Ce-Sn)	3.38

3.2. Photocatalytic Ozonation Tests

Catalytic tests were performed for all prepared films using the following operational parameters: pH = 7, gas flow rate = 10 L/h, temperature = 20 °C, two or four catalytic slides, and two different O₃ concentrations: 6 or 12 g/Nm³ (equivalent to 1 mg/min and 2 mg/min, respectively). For noncatalytic tests, bare glass slides were used. The reactions were repeated once with the same slides for verification of catalysts' reusability and, for all runs, a multiparametric assessment of the process was performed. Thus, several chemical species and parameters were monitored: paracetamol concentration, total organic carbon (TOC), solution absorbance at 254 nm, ammonia ions, and nitrate ions. From the evolution of paracetamol normalized concentrations (Figure 6) it can be observed that for lower ozone input (6 g/Nm³), the noncatalytic process occurs very slow compared with catalytic ones. With the increasing O₃ concentration (12 g/Nm³), the reaction rate for the noncatalytic process rose significantly and became comparable with catalytic tests performed with two catalytic slides (Figure 7a). However, when using four slides (Figure 7b), the oxidation of the pollutant occurs much more rapidly and the target compound is removed in less than 45 min for (Ti) and (Ti-Sn) systems and in nearly 90 min in absence of catalysts. The reusability of catalytic slides is proved for all systems by the same evolution of normalized paracetamol concentration for two consecutive reactions (Figures S2–S5, Supplementary Material). Monitoring the process only from the target pollutant perspective is not a good choice since the oxidation byproducts can also be toxic and require advanced removal. Thus, UV absorbance at 254 nm (UV254) for prelevated samples during the reactions is generally considered as an indicator of the presence of unsaturated carbon bonds (mostly from aromatic compounds) and is a useful monitoring tool [69–76]. Figure 8 shows that the evolution of the aromatic and/or double bond containing oxidation byproducts follows the same behavior such as the removal of the parent compound and is persistent throughout the entire reactions, especially for processes with a low ozone concentration of two catalytic slides. The reason for this is that the paracetamol molecule loses the acetamide group which is further transformed into ammonia ions. Moreover, the core of the molecule is more or less

destroyed (depending on reaction conditions) by consecutive augmentation with oxygen, followed by cycle opening and subsequent transformation in smaller moieties [77–81]. Additionally, this parameter was used to verify the reusability of the catalytic system and it was found that for two consecutive reactions the activity remains unchanged (Figures S6–S9, Supplementary Material). The gradual destruction of pollutant molecules is the reason for the slow mineralization process, as can be observed from Figure 9a–c where TOC/TOC₀ evolution versus time is depicted. The elimination of organic carbon by mineralization is almost absent without catalysts at 6 g O₃/Nm³ m and, in the presence of a catalyst, the TOC removal attains 35%. Doubling the ozone dose and using two catalyst slides lead to TOC elimination and up to 55% for (Ti) and 48% for (Ti-Ce-Sn) thin films, while for noncatalytic reaction, mineralization occurs up to 38%. By using four catalytic slides, mineralization is improved up to ~68% for all systems.

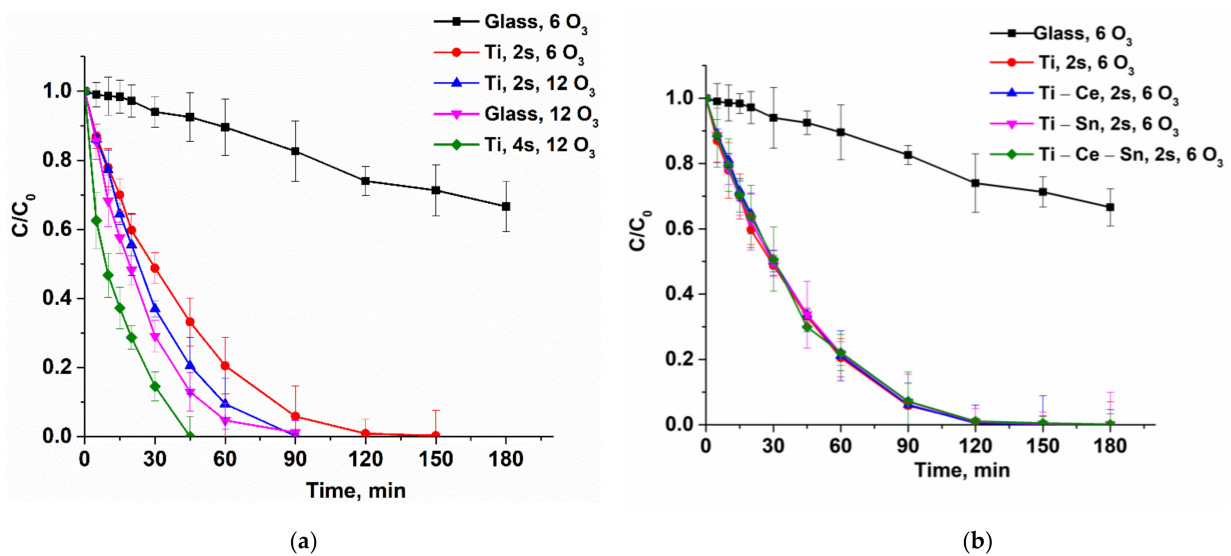


Figure 6. (a) Evolution of paracetamol normalized concentration during the oxidation process for (Ti) system at different ozone concentrations and number of slides; (b) Comparison of prepared catalytic systems at a lower ozone input and two slides.

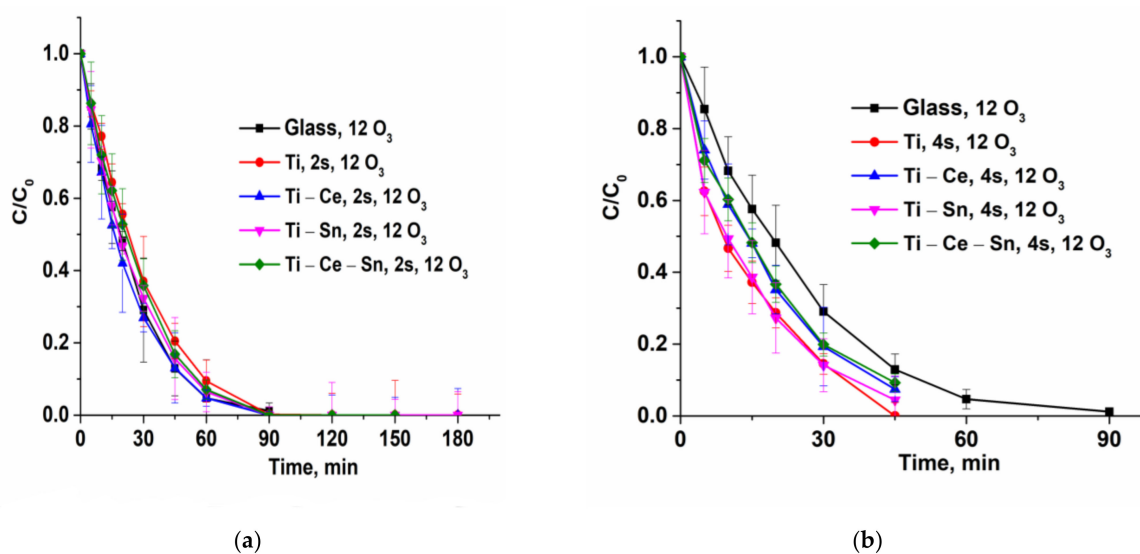


Figure 7. (a) Comparison of prepared catalytic systems at a higher ozone input and two slides; (b) Comparison of prepared catalytic systems at a higher ozone input and four slides.

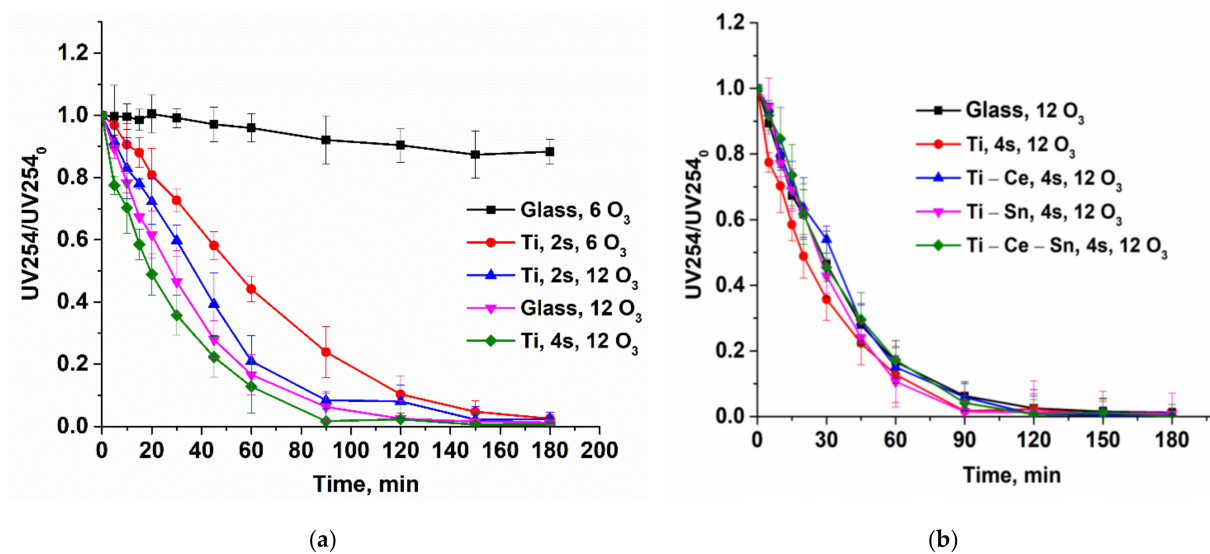


Figure 8. (a) Evolution of normalized UV254 parameter for (Ti) system in different reaction conditions; (b) Evolution of a normalized UV254 parameter for all prepared systems at a higher ozone input and four slides.

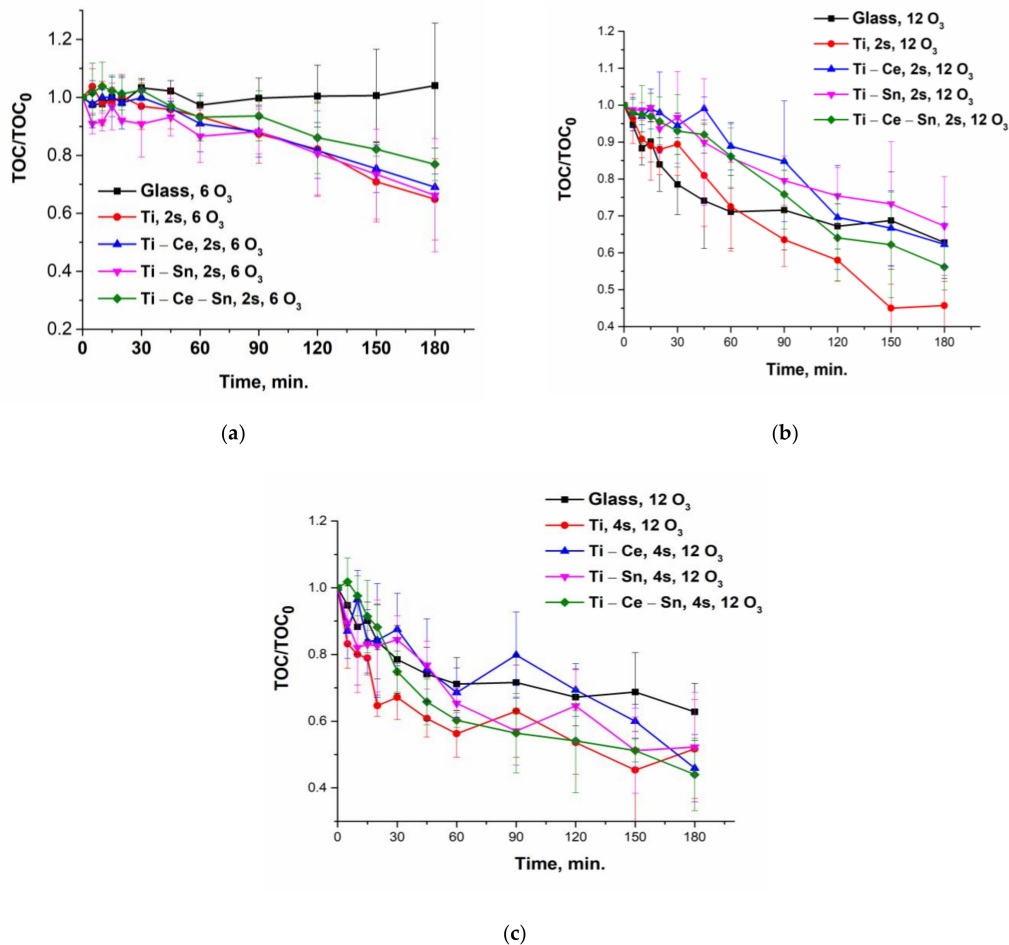


Figure 9. (a) Evolution of normalized TOC for all prepared systems at a lower ozone input and two slides; (b) Evolution of normalized TOC for all prepared systems at a higher ozone input and two slides; (c) Evolution of normalized TOC for all prepared systems at a higher ozone input and four slides.

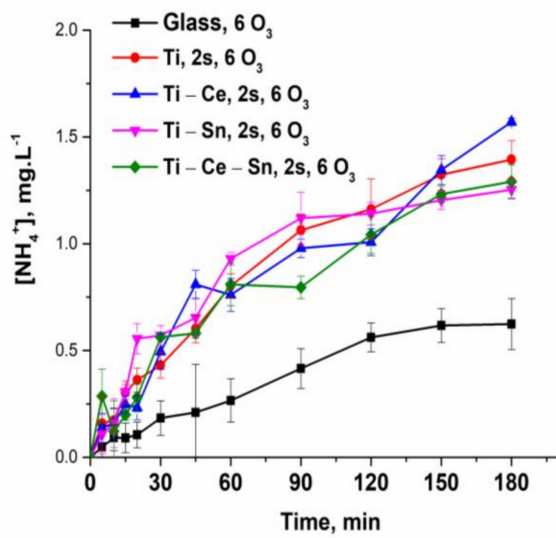
During the oxidation process besides the different organic molecules, another toxic and refractory pollutant is accumulated in the reaction system, namely, ammonia. Ammonia removal represents, in general, a significant challenge due to strict environmental regulations and, the main elimination route is by biological processes which require some demanding conditions to be applied (high capital costs, difficult process monitoring, large to medium effluents volumes, etc.) [82,83]. Catalytic ozonation, due to its flexibility as a process, can overcome these issues and eliminate the noxious ions. The only concern is the formation of nitrate ions but, in this case, the maximum concentration limit is significantly higher than those for ammonia. Hence, from Figure 10a–c presenting the ammonia build-up and subsequent removal, and Figure 11a–c, which shows the formation of nitrate ions, it can be observed that the presence of prepared catalytic systems can eliminate the toxic ions. Thus, for a lower ozone concentration, the amount of ammonia released during the noncatalytic test is much smaller compared to all catalytic systems since the overall process is very slow (not only for ammonia). By doubling the ozone concentration and in absence of a catalyst, the outcome is a higher accumulation of ammonia until some point where the concentration reaches a plateau. On the contrary, for prepared thin films regardless of the number of slides used and ozone concentration, the ammonia is oxidized at a rapid pace, as can be detected from the nitrate formation. However, the most active systems for ammonia removal are (Ti) and (Ti-Ce-Sn).

3.2.1. Ozone Consumption

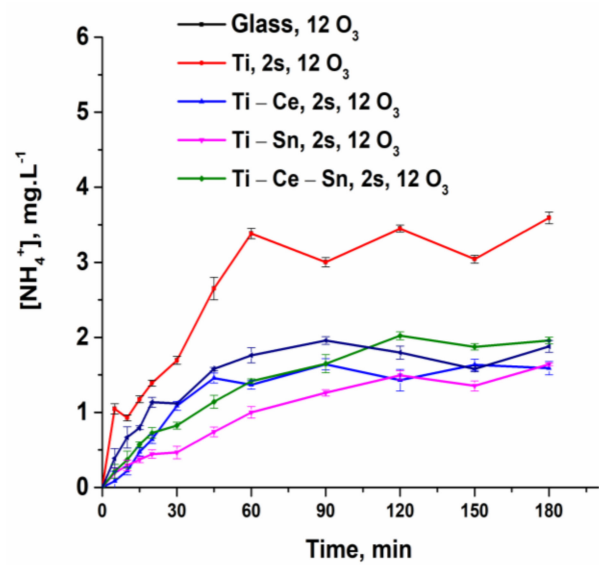
Ozone consumption is an important parameter that governs the efficiency of the process from an economical perspective. Using an online analyzer is a much easier and accurate method to obtain the real ozone consumption compared with the iodometric approach. During a reaction, the amount of ozone that enters the reactor is not entirely consumed and, the residual ozone is lost without the possibility of being recovered. Hence, the main objectives in the oxidation processes are using in large amounts the reactants, and completely removing the organic matter. From Figure 12a–c and Table 3, it can be observed that ozone is efficiently used in the presence of catalysts, even for lower input concentrations of the oxidant agent compared with not-catalytic processes. These values were obtained by integrating the area below the ozone evolution curve using Origin lab software. Additionally, it can be noticed that in terms of TOC removal, (Ti-Ce) and (Ti-Ce-Sn) are the most effective systems with 36.33 and 39.53 mg O₃/mg TOC (for 4 slides) or 15.21 and 12.72 mg O₃/mg TOC removed (for 2 slides).

Table 3. Ozone consumption during the oxidation process for prepared thin films in different conditions.

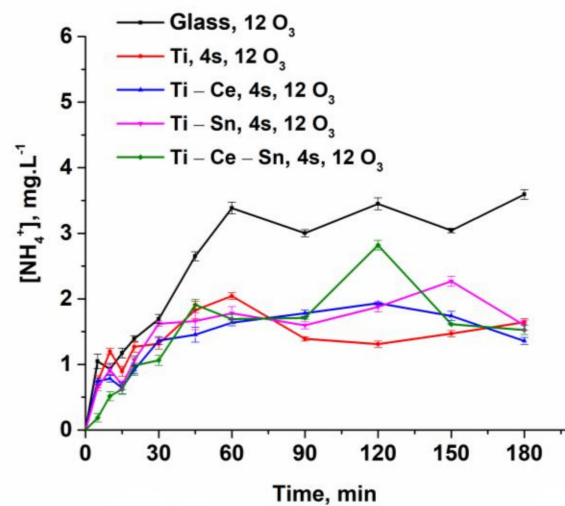
Catalytic System/Ozone Concentration	Consumed Ozone (mg)	Residual Ozone (mg)	Ozone Input (mg)	mgO ₃ /mg TOC Removed (Consumed Ozone)	mgO ₃ /mg TOC Removed (Ozone Input)
Glass, 12 O ₃	261.38	98.62	360	54.10	74.51
Ti, 4s, 12 O ₃	341.85	18.15	360	48.88	51.48
Ti-Ce, 4s, 12 O ₃	254.86	105.14	360	36.44	51.48
Ti-Sn, 4s, 12 O ₃	290.01	69.99	360	47.52	58.98
Ti-Ce-Sn, 4s, 12 O ₃	286.53	73.47	360	39.53	49.67
Ti, 2s, 12 O ₃	324.45	35.55	360	45.57	50.56
Ti-Ce, 2s, 12 O ₃	343.54	16.46	360	67.54	70.78
Ti-Sn, 2s, 12 O ₃	327.26	32.74	360	77.99	85.80
Ti-Ce-Sn, 2s, 12 O ₃	342.22	17.78	360	61.17	64.35
Glass, 6 O ₃	157.34	22.66	180	412.47	471.88
Ti, 2s, 6 O ₃	160.72	19.28	180	33.26	37.25
Ti-Ce, 2s, 6 O ₃	164.79	15.21	180	40.50	44.24
Ti-Sn, 2s, 6 O ₃	155.56	24.44	180	33.98	39.32
Ti-Ce-Sn, 2s, 6 O ₃	167.28	12.72	180	54.82	58.98



(a)

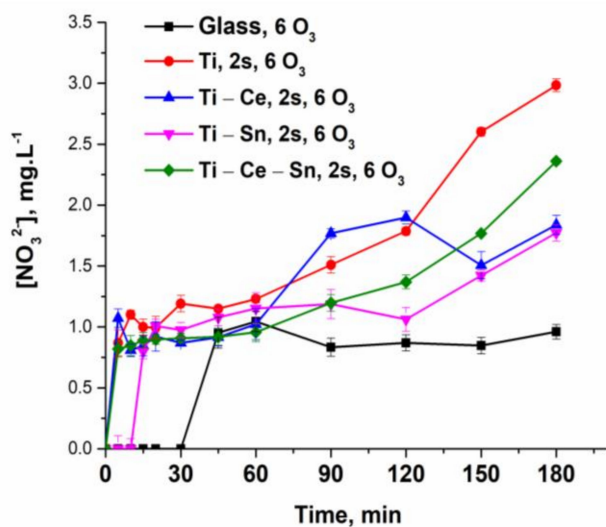


(b)

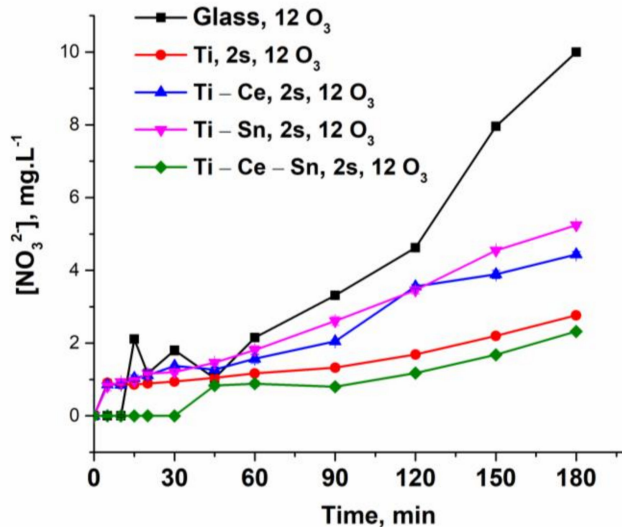


(c)

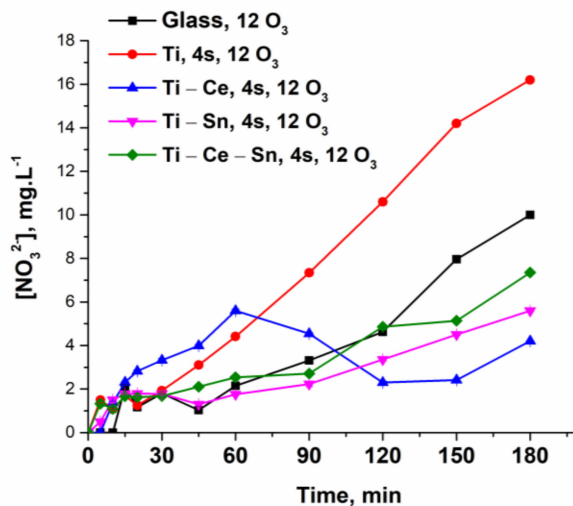
Figure 10. (a) Evolution of ammonia ions for all prepared systems at a lower ozone input and two slides; (b) Evolution of ammonia ions for all prepared systems at a higher ozone input and two slides; (c) Evolution of ammonia ions for all prepared systems at a higher ozone input and four slides.



(a)



(b)



(c)

Figure 11. (a) Evolution of nitrate ions for all prepared systems at a lower ozone input and two slides; (b) Evolution of nitrate ions for all prepared systems at a higher ozone input and two slides; (c) Evolution of nitrate ions for all prepared systems at a higher ozone input and four slides.

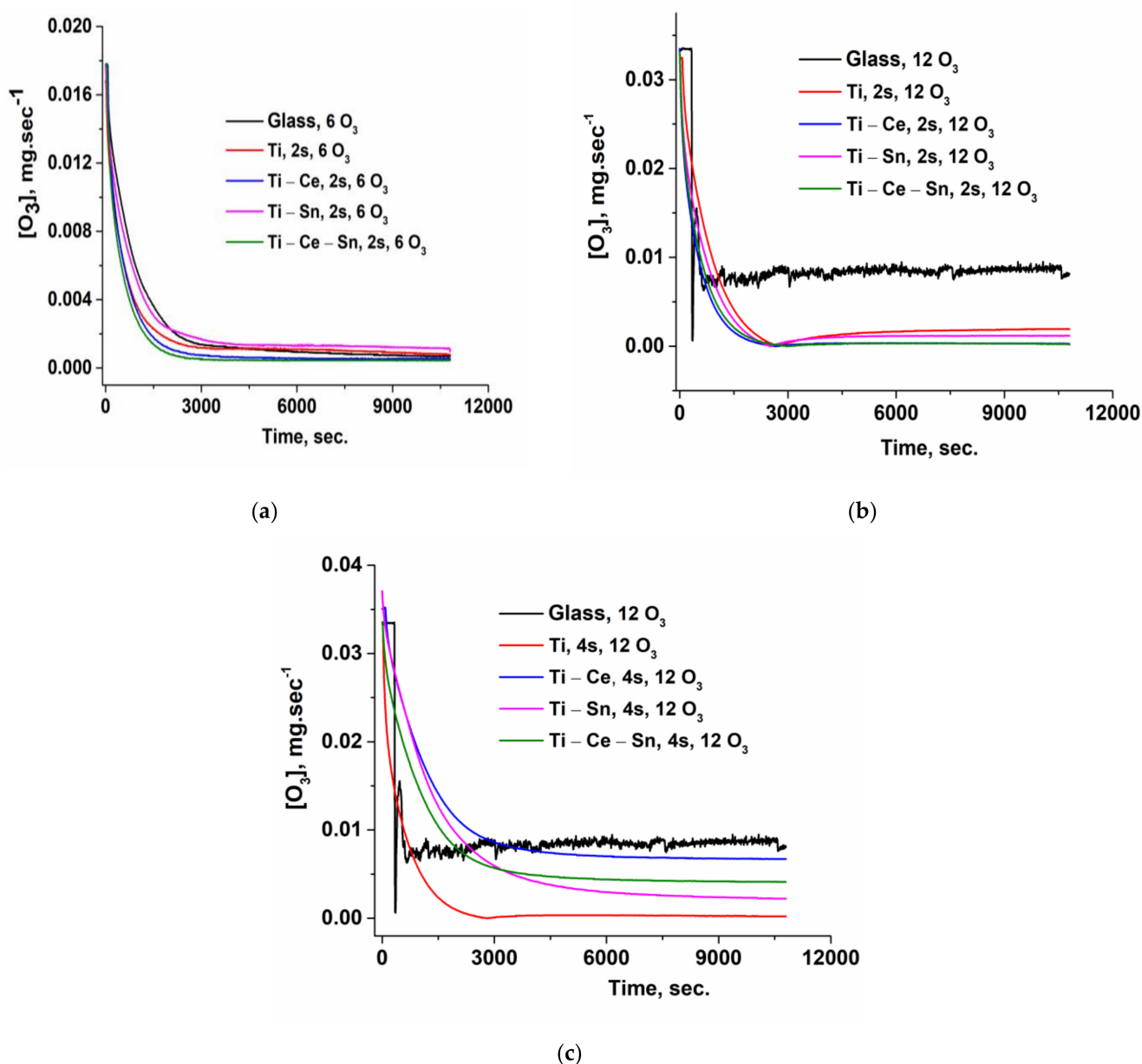


Figure 12. (a) Ozone concentration evolution in time for a lower ozone input and two slides; (b) Ozone concentration evolution in time for a higher ozone input and two slides; (c) Ozone concentration evolution in time for a higher ozone input and four slides.

3.2.2. Kinetic Study

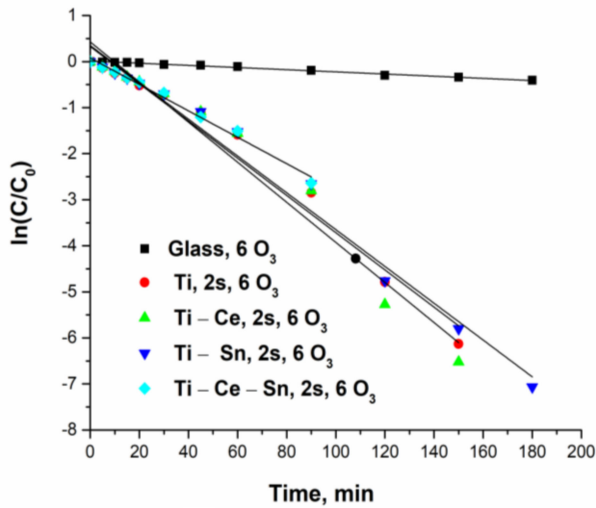
Paracetamol (*Pa*) ozonation in the presence and absence of catalysts can be modeled by a pseudo-first-order kinetic (Equations (2)–(4)) where k_1 and k_2 are the reaction rate constants of pollutant interaction with ozone and $OH\bullet$ respectively. By plotting $\ln[Pa]/[Pa]_0$ versus time (Equation (5), Figure 13a–c), the observed constants ($k_{obs\ cat}$ and $k_{obs\ not-cat}$) will be obtained and are presented in Table 4. The values of the kinetic constants are used as indicators for comparing the performances of catalytic and not-catalytic processes. It can be observed that most active systems are (Ti) and (Ti-Ce-Sn) since their removal rate constant of paracetamol are 1.5 and 1.53 times, respectively, higher than that of the noncatalytic process.

$$-\frac{d[Pa]}{dt} = k_1[O_3][Pa] + k_2[OH\bullet][Pa] = k_{obs\ cat}[Pa] \tag{2}$$

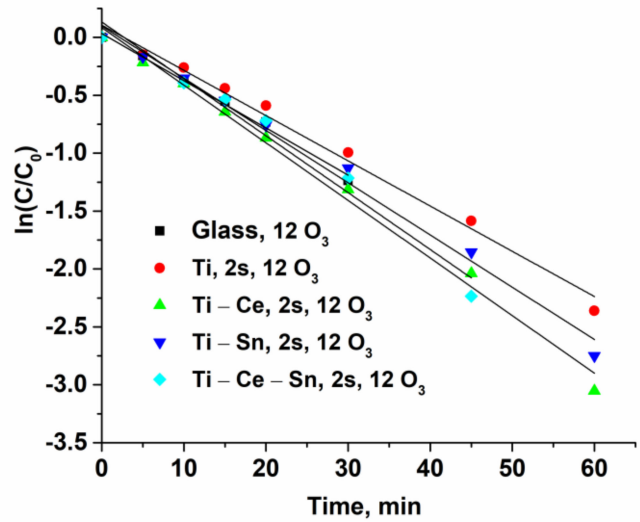


$$-\frac{d[Pa]}{dt} = k_1[O_3][Pa] = k_{obs\ not-cat}[Pa] \tag{4}$$

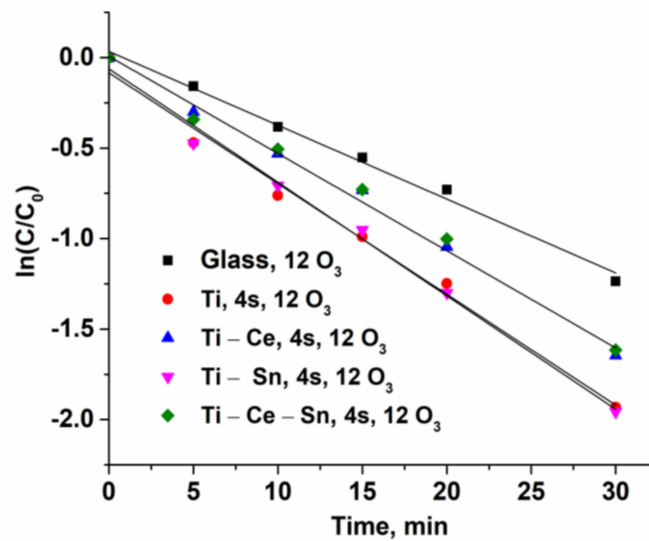
$$\ln\left(\frac{[Pa]}{[Pa]_0}\right) = -k_{obs}t \tag{5}$$



(a)



(b)



(c)

Figure 13. (a) Pseudo-first-order plots of $\ln(C/C_0)$ lower ozone input and two slides; (b) Pseudo-first-order plots of $\ln(C/C_0)$ higher ozone input and two slides; (c) Pseudo-first-order plots of $\ln(C/C_0)$ higher ozone input and four slides.

Table 4. Kinetic parameters for the paracetamol oxidation in different experimental conditions.

Catalytic System/Ozone Concentration	k_{obs} (min^{-1}) 10^2	R^2
Glass, 12 O ₃	4.07	0.9913
Ti, 4s, 12 O ₃	6.12	0.98778
Ti-Ce, 4s, 12 O ₃	5.37	0.99401
Ti-Sn, 4s, 12 O ₃	6.26	0.99085
Ti-Ce-Sn, 4s, 12 O ₃	5.19	0.98929
Ti, 2s, 12 O ₃	3.90	0.98754
Ti-Ce, 2s, 12 O ₃	4.97	0.99081
Ti-Sn, 2s, 12 O ₃	4.51	0.98938
Ti-Ce-Sn, 2s, 12 O ₃	4.91	0.9672
Glass, 6 O ₃	0.23	0.99029
Ti, 2s, 6 O ₃	4.04	0.97132
Ti-Ce, 2s, 6 O ₃	4.35	0.95859
Ti-Sn, 2s, 6 O ₃	3.99	0.98008
Ti-Ce-Sn, 2s, 6 O ₃	2.87	0.98847

3.2.3. Photocatalytic Mechanism

Photocatalytic ozonation of different pollutants generally involves several steps and routes [24,84–90]. In this study, from the reactions at small ozone concentration (6O₃), it can be observed that direct oxidation with ozone (Figure 14A) has low importance (Equations (6) and (7)), while at a higher ozone concentration (12O₃) and in the presence of UV radiation (Figure 14B), the radical production increases significantly (Equations (8)–(10)). In the presence of catalysts, several processes occur. The process starts with electrons transfer from the valence band to the conduction band as a result of radiation excitation. Thus, the formed electrons and holes are available for interaction with O₃ and OH[−]_(s) (Figure 14C,E) (Equations (11)–(16)). All prepared catalytic systems can perform this step as resulted from experimental data. These radicals represent the core of the process by performing the oxidation of paracetamol molecules and leading to complete mineralization of organic substrate (Equations (17) and (18)). As already stated, ammonia is a refractory to oxidation pollutant therefore, require significant amount of radical species depending on reaction conditions [89]. However it can be observed that catalytic systems are able to sustain several parallel processes and eliminating the toxic compounds like ammonia (Figure 14F). Mixed components thin films present some properties which can improve their catalytic activity. Hence in case of (Ti-Sn) system the photogenerated electrons from TiO₂ conduction band migrate into the SnO₂ conduction band while formed holes migrate backwards (Equations (19) and (20)) [90]. This is an important step in delaying the recombination of electrons and holes. In case of (Ti-Ce) system two significant phenomena occur: on CeO₂ oxide surface some oxygen vacancies are formed through interaction with oxygen species from gas/liquid phase and a redox couple Ce³⁺/Ce⁴⁺ (Figure 14D) is formed [91,92]. Furthermore, Ce³⁺ is able to generate radicalic species in a similar manner with electrons from the conductive band (Equations (21) and (22)); a transfer of electrons from CeO₂ also occurs conduction band to TiO₂ conduction band since bandgap energy of CeO₂ is situated at more negative values (−0.37 eV) than those of TiO₂ (−0.24 eV) while holes migrate in opposite directions (Equations (23) and (24)) [92]. Hence, (Ti-Ce-Sn) system apart from a slower recombination of charges may be subject to electron agglomeration in SnO₂ conduction band and of holes in CeO₂ valence band.

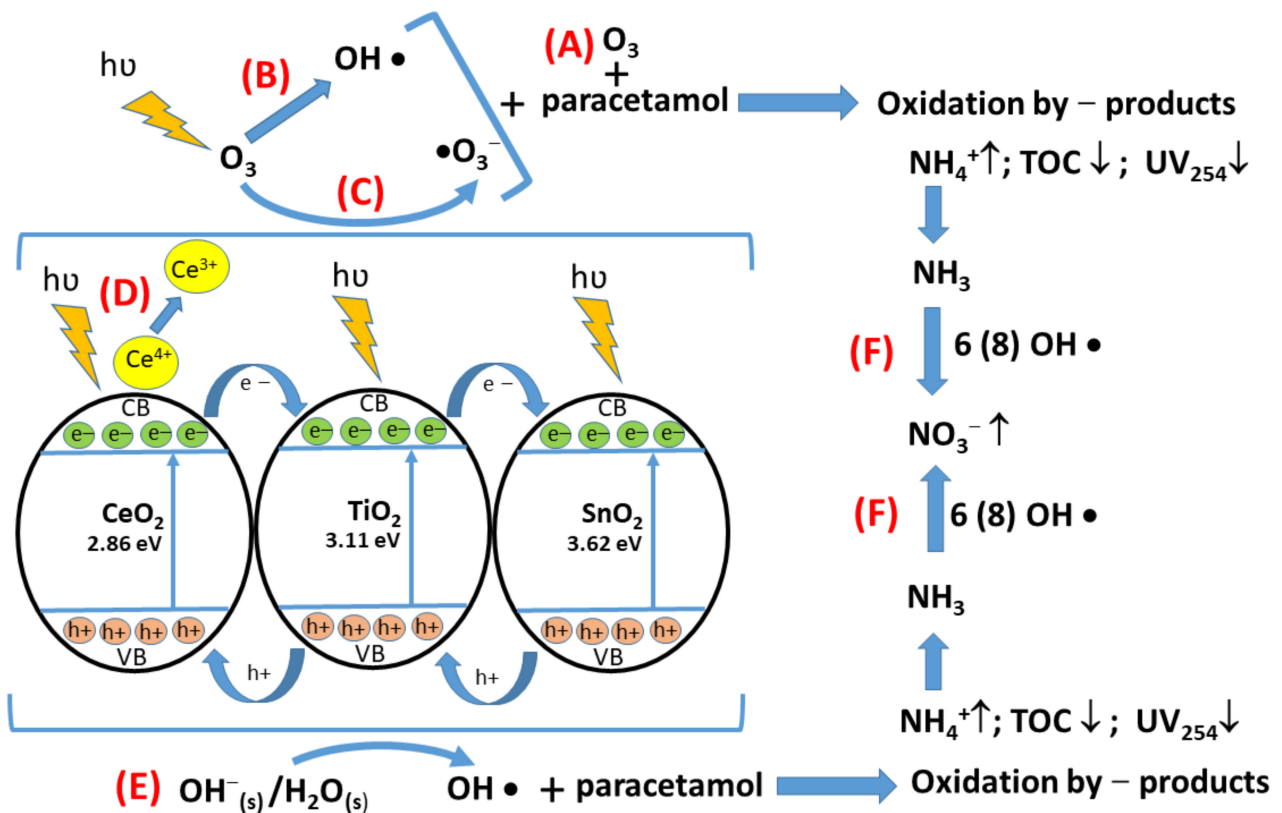
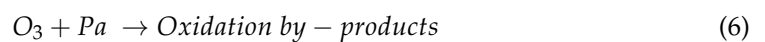
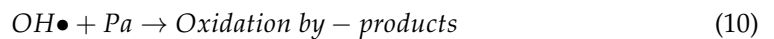
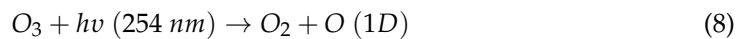


Figure 14. Proposed photocatalytic mechanism for paracetamol oxidation; occurring processes: direct oxidation with ozone (A); radical production in the presence of UV radiation (B); interactions of formed electrons and holes with O_3 and OH (C,E); $\text{Ce}^{3+}/\text{Ce}^{4+}$ formation (D), NH_3 oxidation (F).

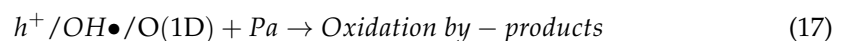
O_3 direct reactions:

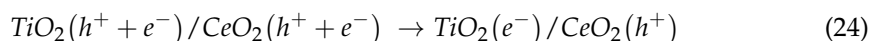
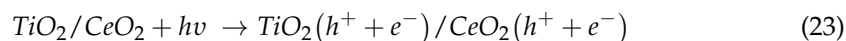
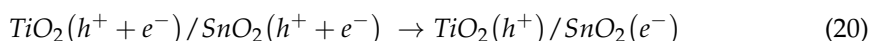
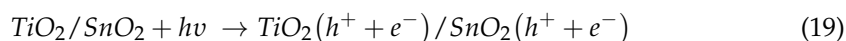


O_3/UV reactions:



$\text{O}_3/\text{UV}/\text{catalyst}$ reactions:





4. Conclusions

For several years, catalytic ozonation represents an important alternative for water treatment. Therefore, intensive work was made in order to improve this process. In this study, paracetamol (a widely used NSAID) catalytic ozonation using $\text{TiO}_2\text{-Me}_x\text{O}_y$ thin films was investigated. Using thin film in the oxidation removal of pollutants represents an important step for enhancement for this type of process and, in addition, to its simplification by avoiding the difficult step of catalyst separation. The present study describes for the first time in literature, the removal of paracetamol from aqueous solutions using thin films catalysts based on $\text{TiO}_2\text{-Me}_x\text{O}_y$ nanosystems deposited on glass plates and immersed into a semi-batch reactor; the prepared thin films being very active in eliminating the targeted compound.

Considering that the initial concentration of the pollutant selected for this study is much higher compared with real-world effluents, the obtained results are very encouraging, giving the prospect of the complete elimination of the pollutants from aqueous effluents regardless of the compound type. The relative performances of noncatalytic processes can be attributed mainly to the presence of UV radiation since it is well-known that ozonation alone cannot cope with some resistance to oxidation chemical species. The higher than usual input concentrations represent a successful endurance test for the prepared catalytic systems.

Supplementary Materials: The following supporting information can be downloaded at: <https://www.mdpi.com/article/10.3390/nano12040613/s1>, Figure S1: FTIR spectra of prepared film before and after use in oxidation reaction; Figure S2: Evolution of paracetamol normalized concentration during the oxidation process for (Ti) system for two successive cycles at lower ozone concentrations and 2 number of slides; Figure S3: Evolution of paracetamol normalized concentration during the oxidation process for (Ti-Ce) system for two successive cycles at lower ozone concentrations and 2 number of slides; Figure S4: Evolution of paracetamol normalized concentration during the oxidation process for (Ti-Sn) system for two successive cycles at lower ozone concentrations and 2 number of slides; Figure S5: Evolution of paracetamol normalized concentration during the oxidation process for (Ti-Ce-Sn) system for two successive cycles at lower ozone concentrations and 2 number of slides; Figure S6: Evolution of normalized UV254 parameter during the oxidation process for (Ti) system for two successive cycles at lower ozone concentrations and 2 number of slides; Figure S7: Evolution of normalized UV254 parameter during the oxidation process for (Ti-Ce) system for two successive cycles at lower ozone concentrations and 2 number of slides; Figure S8: Evolution of normalized UV254 parameter during the oxidation process for (Ti-Ce) system for two successive cycles at lower ozone concentrations and 2 number of slides; Figure S9: Evolution of normalized UV254 parameter during the oxidation process for (Ti-Ce) system for two successive cycles at lower ozone concentrations and 2 number of slides.

Author Contributions: Conceptualization, S.M.A., I.F., R.C.F. and A.D.; methodology, S.M.A., R.C.F. and A.D.; validation, S.M.A., I.F. and R.C.F.; investigation, S.M.A., R.I.B., A.V.N., C.B., E.A.O., M.N.V. and S.U.; resources, S.M.A., I.F., R.C.F. and S.U.; data curation, S.M.A., I.F. and R.C.F.; writing—original draft preparation, S.M.A., I.F., R.C.F. and A.D.; writing—review and editing, S.M.A., I.F., R.C.F. and A.D.; visualization, S.M.A. and I.F.; supervision, S.M.A., I.F. and R.C.F.; project administration, S.M.A., I.F. and S.U.; funding acquisition, S.M.A., I.F. and S.U. All authors have read and agreed to the published version of the manuscript.

Funding: This research was funded through a grant from the Romanian National Authority for Scientific Research and Innovation, CNCS/CCCDI-UEFISCDI, project GreenCatOx, project code PN-III-P2-2.1-PED-2019-3166, contract 299/2020, within PNCDI III. IF, RCF and RIB also acknowledge the financial support of the Romanian Ministry of Research and Innovation, MCI (Ministry of Research, Innovation, and Digitization, MCID) through INCDCP ICECHIM Bucharest 2019–2022 Core Program PN. 19.23—Chem-Ergent, Project No.19.23.03. The APC was funded by project GreenCatOx, project code PN-III-P2-2.1-PED-2019-3166, contract 299/2020, within PNCDI III.

Institutional Review Board Statement: Not applicable.

Informed Consent Statement: Not applicable.

Data Availability Statement: All data are available upon reasonable request from the authors.

Conflicts of Interest: The authors declare no conflict of interest.

References

1. Santos, L.; Araújo, A.N.; Fachini, A.; Pena, A.; Delerue-Matos, C.; Montenegro, M. Ecotoxicological Aspects Related to the Presence of Pharmaceuticals in the Aquatic Environment. *J. Hazard. Mat.* **2009**, *175*, 45–95. [CrossRef] [PubMed]
2. Persson, M.; Sabelström, E.; Gunnarsson, B. Handling of unused prescription drugs—Knowledge, behaviour and attitude among Swedish people. *Environ. Int.* **2008**, *35*, 771–774. [CrossRef] [PubMed]
3. Li, D.; Yang, M.Y.; Hu, J.; Ren, L.; Zhang, Y.; Li, K. Determination and fate of oxytetracycline and related compounds in oxytetracycline production wastewater and the receiving river. *Environ. Toxicol. Chem.* **2008**, *27*, 80–86. [CrossRef] [PubMed]
4. Gomez Ramos, M.J.; Petrovic, M.; Fernández-Alba, A.; Barcelo, D. Determination of Pharmaceuticals of Various Therapeutic Classes by Solid-Phase Extraction and Liquid Chromatography-Tandem Mass Spectrometry Analysis in Hospital Effluent Wastewaters. *J. Chromatogr. A* **2006**, *1114*, 224–233. [CrossRef]
5. Aitken, M.; Kleinrock, M. Global Medicines Use in 2020. Outlook and Implications. Available online: <https://www.iqvia.com/-/media/iqvia/pdfs/institute-reports/global-medicines-use-in-2020> (accessed on 18 December 2021).
6. Hughes, S.; Kay, P.; Brown, L. Global Synthesis and Critical Evaluation of Pharmaceutical Data Sets Collected from River Systems. *Environ. Sci. Technol.* **2012**, *47*, 661–677. [CrossRef]
7. Braun, P.; Lange, F.; Schrader, S.; Lorenz, W. Determination of Endocrine Disrupting Compounds and Acidic Drugs in Water by Coupling of Derivatization, Gas Chromatography and Negative-Chemical Ionization Mass Spectrometry. *Clean* **2007**, *35*, 444–451. [CrossRef]
8. Cleuvers, M. Mixture Toxicity of the Anti-Inflammatory Drugs Diclofenac, Ibuprofen, Naproxen, and Acetylsalicylic Acid. *Ecotoxicol. Environ. Saf.* **2004**, *59*, 309–315. [CrossRef]
9. RFDTV, PAP and Paracetamol Market Size In 2021: Top Countries Data with 2.0% CAGR, Global Industry Brief Analysis by Top Key companies and Growth Insights to 2027. Latest 136 Pages Report. Available online: <https://www.rfdtv.com/story/44670147/pap-and-paracetamol-market-size-in-2021-top-countries-data-with-20-cagr-global-industry-brief-analysis-by-top-key-companies-and-growth-insights-to> (accessed on 19 December 2021).
10. Al-Kaf, A.G.; Naji, K.M.; Abdullah, Q.Y.M.; Edrees, W.H.A. Occurrence of Paracetamol in Aquatic Environments and Transformation by Microorganisms: A Review. *Chron. Pharm. Sci.* **2017**, *1*, 341–355.
11. Zhang, Z.; Lin, F.; Xiang, L.; Yu, H.; Wang, Z.; Yan, B.; Chen, G. Synergistic effect for simultaneously catalytic ozonation of chlorobenzene and NO over MnCoO catalysts: Byproducts formation under practical conditions. *Chem. Eng. J.* **2022**, *427*, 130929. [CrossRef]
12. Yuan, Y.; Garg, S.; Wang, Y.; Li, W.; Chen, G.; Gao, M.; Zhong, J.; Wang, J.; Waite, T.D. Influence of salinity on the heterogeneous catalytic ozonation process: Implications to treatment of high salinity wastewater. *J. Hazard. Mat.* **2022**, *423*, 127255. [CrossRef]
13. Wang, Z.; Xian, W.; Ma, Y.; Xu, T.; Jiang, R.; Zhu, H.; Mao, X. Catalytic ozonation with disilicate-modified nZVI for quinoline removal in aqueous solution: Efficiency and heterogeneous reaction mechanism. *Sep. Purif. Technol.* **2022**, *281*, 119961. [CrossRef]
14. Shao, S.; Li, Z.; Gao, K.; Zhang, J.; Liu, Y.; Jiao, W. Preparation of Cu-MnO_x/γ-Al₂O₃ by high gravity-assisted impregnation method for heterogeneous catalytic ozonation of nitrobenzene. *Sep. Purif. Technol.* **2022**, *280*, 119896. [CrossRef]
15. Kohantorabi, M.; Moussavi, G.; Oulego, P.; Giannakis, S. Heterogeneous catalytic ozonation and peroxone-mediated removal of Acetaminophen using natural and modified hematite-rich soil, as efficient and environmentally friendly catalysts. *Appl. Catal. B Environ.* **2022**, *301*, 120786. [CrossRef]
16. Heidari, Z.; Pelalak, R.; Eshaghi Malekshah, R.; Pishnamazi, M.; Rezakazemi, M.; Aminabhavi, T.M.; Shirazian, S. A new insight into catalytic ozonation of sulfasalazine antibiotic by plasma-treated limonite nanostructures: Experimental, modeling and mechanism. *Chem. Eng. J.* **2022**, *428*, 131230. [CrossRef]
17. Guan, Z.; Guo, Y.; Huang, Z.; Liao, X.; Chen, S.; Ou, X.; Sun, S.; Liang, J.; Cai, Y.; Xie, W.; et al. Simultaneous and efficient removal of organic Ni and Cu complexes from electroless plating effluent using integrated catalytic ozonation and chelating precipitation process in a continuous pilot-scale system. *Chem. Eng. J.* **2022**, *428*, 131250. [CrossRef]
18. Zuo, X.; Ma, S.; Wu, Q.; Xiong, J.; He, J.; Ma, C.; Chen, Z. Nanometer CeO₂ doped high silica ZSM-5 heterogeneous catalytic ozonation of sulfamethoxazole in water. *J. Hazard. Mater.* **2021**, *411*, 125072. [CrossRef]

19. Zhang, Z.; Ai, H.; Fu, M.-L.; Hu, Y.-b.; Liu, J.; Ji, Y.; Vasanthakumar, V.; Yuan, B. A new insight into catalytic ozonation of ammonia by MgO/Co₃O₄ composite: The effects, reaction kinetics and mechanism. *Chem. Eng. J.* **2021**, *418*, 129461. [[CrossRef](#)]
20. Zhang, J.; Xin, B.; Shan, C.; Zhang, W.; Dionysiou, D.D.; Pan, B. Roles of oxygen-containing functional groups of O-doped g-C₃N₄ in catalytic ozonation: Quantitative relationship and first-principles investigation. *Appl. Catal. B Environ.* **2021**, *292*, 120155. [[CrossRef](#)]
21. Zhang, F.; Liao, J.; Lu, J.; Niu, J. Extensive incorporation of carboxyl groups into g-C₃N₄ by integrated oxygen doping and HNO₃ oxidation for enhanced catalytic ozonation of para-chlorobenzoic acid and atrazine. *Sep. Purif. Technol.* **2021**, *256*, 117806. [[CrossRef](#)]
22. Tang, X.; Zhang, Y.; Li, W.; Geng, J.; Ren, H.; Xu, K. Mechanism and toxicity evaluation of catalytic ozonation over Cu/Ce-Al₂O₃ system aiming at degradation of humic acid in real wastewater. *Sci. Rep.* **2021**, *11*, 8748. [[CrossRef](#)]
23. Sun, Z.; Ma, J.; Liu, Y.; Wang, H.; Cao, W.; Zhu, N.; Lou, Z. Mineralization of refractory organics in oil refinery wastewater by the catalytic ozonation with magnetic praseodymium-catalysts: Catalytic performances and mechanisms. *Sep. Purif. Technol.* **2021**, *277*, 119506. [[CrossRef](#)]
24. Suligoj, A.; Kete, M.; Cernigoj, U.; Fresno, F.; Lavrencic Stangar, U. Synergism in TiO₂ photocatalytic ozonation for the removal of dichloroacetic acid and thiocloprid. *Environ. Res.* **2021**, *197*, 110982. [[CrossRef](#)]
25. Song, J.; Ma, N.; Chen, W.; Chen, J.; Dai, Q. Insights into mechanism of catalytic ozonation of cinnamyl alcohol over core-shell Fe₃O₄@SiO₂@La₂O₃ catalyst. *Sep. Purif. Technol.* **2021**, *282*, 119969. [[CrossRef](#)]
26. Ren, H.; Wang, Z.; Chen, X.; Jing, Z.; Qu, Z.; Huang, L. Effective mineralization of p-nitrophenol by catalytic ozonation using Ce-substituted La_{1-x}Ce_xFeO₃ catalyst. *Chemosphere* **2021**, *285*, 131473. [[CrossRef](#)]
27. Rashidashmagh, F.; Doekhi-Bennani, Y.; Tizghadam-Ghazani, M.; van der Hoek, J.P.; Mashayekh-Salehi, A.; Heijman, B.; Yaghmaeian, K. Synthesis and characterization of SnO₂ crystalline nanoparticles: A new approach for enhancing the catalytic ozonation of acetaminophen. *J. Hazard. Mater.* **2021**, *404*, 124154. [[CrossRef](#)]
28. Psaltou, S.; Kaprara, E.; Triantafyllidis, K.; Mitrakas, M.; Zouboulis, A. Heterogeneous catalytic ozonation: The significant contribution of PZC value and wettability of the catalysts. *J. Environ. Chem. Eng.* **2021**, *9*, 106173. [[CrossRef](#)]
29. Mu, J.; Li, S.; Wang, J.; Li, X.; Chen, W.; Tong, X.; Tang, Y.; Li, L. Efficient catalytic ozonation of bisphenol A by three-dimensional mesoporous CeO_x-loaded SBA-16. *Chemosphere* **2021**, *278*, 130412. [[CrossRef](#)]
30. Meng, F.; Guo, L.; He, J.; Wang, Z.; Ma, Z.; Zeng, Y.; Zhang, S.; Zhong, Q. V₂O₅-(NH₄)₂V₆O₁₆·1.5H₂O composite catalysts as novel platforms for high-efficiency catalytic ozonation of NO under low temperature. *J. Phys. Chem. Solids* **2021**, *155*, 110112. [[CrossRef](#)]
31. Zhao, Y.; An, H.; Dong, G.; Feng, J.; Ren, Y.; Wei, T. Elevated removal of di-n-butyl phthalate by catalytic ozonation over magnetic Mn-doped ferrosphal ZnFe₂O₄ materials: Efficiency and mechanism. *Appl. Surf. Sci.* **2020**, *505*, 144476. [[CrossRef](#)]
32. Zhang, H.; He, Y.; Lai, L.; Yao, G.; Lai, B. Catalytic ozonation of Bisphenol A in aqueous solution by Fe₃O₄-MnO₂ magnetic composites: Performance, transformation pathways and mechanism. *Sep. Purif. Technol.* **2020**, *245*, 116449. [[CrossRef](#)]
33. Chávez, A.M.; Solís, R.R.; Beltrán, F.J. Magnetic graphene TiO₂-based photocatalyst for the removal of pollutants of emerging concern in water by simulated sunlight aided photocatalytic ozonation. *Appl. Catal. B Environ.* **2020**, *262*, 118275. [[CrossRef](#)]
34. Chávez, A.M.; Quiñones, D.H.; Rey, A.; Beltrán, F.J.; Álvarez, P.M. Simulated solar photocatalytic ozonation of contaminants of emerging concern and effluent organic matter in secondary effluents by a reusable magnetic catalyst. *Chem. Eng. J.* **2020**, *398*, 125642. [[CrossRef](#)]
35. Asgari, E.; Farzadkia, M.; Esrafil, A.; Badi, M.Y.; Jokandan, S.F.; Sobhi, H.R. Application of a photocatalytic ozonation process using TiO₂ magnetic nanoparticles for the removal of Cefazidime from aqueous solutions: Evaluation of performance, comparative study and mechanism. *Optik* **2020**, *212*, 164667. [[CrossRef](#)]
36. Orge, C.A.; Soares, O.S.G.P.; Ramalho, P.S.F.; Pereira, M.F.R.; Faria, J.L. Magnetic Nanoparticles for Photocatalytic Ozonation of Organic Pollutants. *Catalysts* **2019**, *9*, 703. [[CrossRef](#)]
37. Yusuf, M.A.; Abidin, K.; Eliyana, A.; Malago, J.D.; Noor, F.A.; Winata, T. Nickel thin film preparation and its characterization as catalyst for HWC-in plasma-PECVD-growth graphene. *Mat. Today Proc.* **2021**, *44*, 3420–3425. [[CrossRef](#)]
38. Hosseini, A.; Karimi, H.; Foroughi, J.; Sabzehmeidani, M.M.; Ghaedi, M. Heterogeneous photoelectro-Fenton using ZnO and TiO₂ thin film as photocatalyst for photocatalytic degradation Malachite Green. *Appl. Surf. Sci. Adv.* **2021**, *6*, 100126. [[CrossRef](#)]
39. Zhang, X.; Ptasinska, S. Dissociative adsorption of H₂O onto a Pt thin film in direct contact with GaN (0001): Effect of electronic communications between catalyst and a semiconducting support. *Appl. Surf. Sci.* **2020**, *516*, 146127. [[CrossRef](#)]
40. Mauraya, A.K.; Mahana, D.; Pal, P.; Muthiah, S.; Singh, P.; Muthusamy, S.K. Effect of bulk and surface modification of SnO₂ thin films with PdO catalyst on CO gas sensing characteristics prepared by vacuum evaporation process. *J. Alloys Compd.* **2020**, *843*, 155979. [[CrossRef](#)]
41. Sankarasubramanian, K.; Babu, K.J.; Soundarajan, P.; Logu, T.; Gnanakumar, G.; Ramamurthi, K.; Sethuraman, K.; Senthil Kumar, S.M. A new catalyst Ti doped CdO thin film for non-enzymatic hydrogen peroxide sensor application. *Sens. Actuators B Chem.* **2019**, *285*, 164–172. [[CrossRef](#)]
42. Tyagi, P.; Sharma, A.; Tomar, M.; Gupta, V. SnO₂ thin film sensor having NiO catalyst for detection of SO₂ gas with improved response characteristics. *Sens. Actuators B Chem.* **2017**, *248*, 998–1005. [[CrossRef](#)]
43. Li, Y.; Song, W.; Liu, J.; Zhao, Z.; Gao, M.; Wei, Y.; Wang, Q.; Deng, J. The protection of CeO₂ thin film on Cu-SAPO-18 catalyst for highly stable catalytic NH₃-SCR performance. *Chem. Eng. J.* **2017**, *330*, 926–935. [[CrossRef](#)]

44. Fatahpour, M.; Noori Sadeh, F.; Hazeri, N.; Maghsoodlou, M.T.; Hadavi, M.S.; Mahnaei, S. Ag/TiO₂ nano-thin films as robust heterogeneous catalyst for one-pot, multi-component synthesis of bis (pyrazol-5-ol) and dihydropyrano[2,3-c]pyrazole analogs. *J. Saudi Chem. Soc.* **2017**, *21*, 998–1006. [[CrossRef](#)]
45. Kim, S.; Chang, H.-K.; Kim, K.B.; Kim, H.-J.; Lee, H.-N.; Park, T.J.; Park, Y.M. Highly Porous SnO₂/TiO₂ Heterojunction Thin-Film Photocatalyst Using Gas-Flow Thermal Evaporation and Atomic Layer Deposition. *Catalysts* **2021**, *11*, 1144. [[CrossRef](#)]
46. Zhao, W.; Yang, X.; Liu, C.; Qian, X.; Wen, Y.; Yang, Q.; Sun, T.; Chang, W.; Liu, X.; Chen, Z. Facile Construction of All-Solid-State Z-Scheme g-C₃N₄/TiO₂ Thin Film for the Efficient Visible-Light Degradation of Organic Pollutant. *Nanomaterials* **2020**, *10*, 600. [[CrossRef](#)]
47. Nicosia, A.; Vento, F.; Di Mari, G.M.; D'Urso, L.; Mineo, P.G. TiO₂-Based Nanocomposites Thin Film Having Boosted Photocatalytic Activity for Xenobiotics Water Pollution Remediation. *Nanomaterials* **2021**, *11*, 400. [[CrossRef](#)]
48. Stathatos, E.; Lianos, P.; Tsakiroglou, C. Highly efficient nanocrystalline titania films made from organic/inorganic nanocomposite gels. *Micropor. Mesopor. Mat.* **2004**, *75*, 255–260. [[CrossRef](#)]
49. Zheng, Z.; Ng, Y.H.; Tang, Y.; Li, Y.; Chen, W.; Wang, J.; Li, X.; Li, L. Visible-light-driven photoelectrocatalytic activation of chloride by nanoporous MoS₂@BiVO₄ photoanode for enhanced degradation of bisphenol A. *Chemosphere* **2020**, *263*, 128279. [[CrossRef](#)]
50. Pinar Gokdemir, F.; Ece Yuzbasioglu, V.; Keskin, B.; Ozdemir, O.; Kutlu, K. Formation of TiO₂ Thin Films by a Modified Sol-gel Route and Characterization of Structural, Optical and Electrochromic Properties. *Adv. Mat. Lett.* **2014**, *5*, 367–371. [[CrossRef](#)]
51. Haider, A.J.; Thamir, A.D.; Najim, A.A.; Ali, G.A. Improving Efficiency of TiO₂:Ag/Si Solar Cell Prepared by Pulsed Laser Deposition. *Plasmonics* **2016**, *12*, 105–115. [[CrossRef](#)]
52. Thamaphat, K.; Limsuwan, P.; Ngotawornchai, B. Phase characterization of TiO₂ powder by XRD and TEM. *Kasetsart J.* **2008**, *42*, 357–361.
53. Ba-Abbad, M.; Kadhum, A.; Mohamad, A.B.; Takriff, M.; Sopian, K. Synthesis and Catalytic Activity of TiO₂ Nanoparticles for Photochemical Oxidation of Concentrated Chlorophenols under Direct Solar Radiation. *Int. J. Electrochem. Sci.* **2012**, *7*, 4871–4888.
54. Avciata, O.; Benli, Y.; Gördük, S.; Gördük, Ö. Ag doped TiO₂ nanoparticles prepared by hydrothermal method and coating of the nanoparticles on the ceramic pellets for photocatalytic study: Surface properties and photoactivity. *J. Eng. Technol. Appl. Sci.* **2016**, *1*, 34–50. [[CrossRef](#)]
55. Wei, C.H.; Tang, X.H.; Liang, J.R.; Tan, S.Y. Preparation, characterization and photocatalytic activities of boron- and cerium-codoped TiO₂. *J. Environ. Sci.* **2007**, *19*, 90–96. [[CrossRef](#)]
56. Hassan, M.S.; Amna, T.; Al-Deyab, S.S.; Kim, H.C.; Oh, T.H.; Khil, M.S. Toxicity of Ce₂O₃/TiO₂ composite nanofibers against *S. aureus* and *S. typhimurium*: A novel electrospun material for disinfection of food pathogens. *Colloids Surf. A Physicochem. Eng. Asp.* **2012**, *415*, 268–273. [[CrossRef](#)]
57. Patel, S.B.; Radevski, N.; Mondinos, N.; Zhao, X.; Jack, K.; Veder, J.P.; Zhou, Z.F.; Jiang, Z.T. A mechanical and modelling study of magnetron sputtered cerium-titanium oxide film coatings on Si (100). *Ceram. Int.* **2019**, *45*, 6875–6884. [[CrossRef](#)]
58. Duan, N.; Lin, H.; Li, L.; Hu, J.; Bi, L.; Lu, H.; Weng, X.; Xie, J.; Deng, L. ZrO₂-TiO₂ thin films: A new material system for mid-infrared integrated photonics. *Opt. Mater. Express* **2013**, *3*, 1537–1545. [[CrossRef](#)]
59. Lubas, M.; Jasinski, J.J.; Sitarz, M.; Kurpaska, L.; Podsiad, P.; Jasinski, J. Raman spectroscopy of TiO₂ thin films formed by hybrid treatment for biomedical applications. *Spectrochim Acta A Mol. Biomol. Spectrosc.* **2014**, *133*, 867–871. [[CrossRef](#)]
60. Balzano, V.; Cavaliere, E.; Fanetti, M.; Gardonio, S.; Gavioli, L. The Role of Substrate on Thermal Evolution of Ag/TiO₂ Nanogranular Thin Films. *Nanomaterials* **2021**, *11*, 2253. [[CrossRef](#)]
61. Medjaldi, F.; Bouabellou, A.; Bouachiba, Y.; Taabouche, A.; Bouatia, K.; Serrar, H. Study of TiO₂, SnO₂ and nanocomposites TiO₂:SnO₂ thin films prepared by sol-gel method: Successful elaboration of variable-refractive index systems. *Mat. Res. Express* **2020**, *7*, 016439. [[CrossRef](#)]
62. Topuz, B.B.; Gündüz, G.; Mavis, B.; Çolak, Ü. The effect of tin dioxide (SnO₂) on the anatase-rutile phase transformation of titania (TiO₂) in mica-titania pigments and their use in paint. *Dyes Pigm.* **2011**, *90*, 123–128. [[CrossRef](#)]
63. Mosquera, A.A.; Albella, J.M.; Navarro, V.; Bhattacharyya, D.; Endrino, J.L. Effect of silver on the phase transition and wettability of titanium oxide films. *Sci. Rep.* **2016**, *6*, 32171. [[CrossRef](#)] [[PubMed](#)]
64. Kabir, I.; Sheppard, L.; Shhamiri, R.; Koshy, P.; Liu, R.; Joe, W.; Le, A.; Lu, X.; Chen, W.F.; Sorrell, C. Correction to: Contamination of TiO₂ thin films spin coated on borosilicate and rutile substrates. *J. Mat. Sci.* **2021**, *56*, 18341–18343. [[CrossRef](#)]
65. Singhal, A.; Ebrahimi, F.; Hosseini, S. A comprehensive review on the modeling of smart piezoelectric structures. *Struct. Eng. Mech.* **2020**, *74*, 611–633.
66. Olkun, A.; Pat, S.; Akkurt Özgür, N.; Mohammadigharehbagh, R.; Demirkol, U.; Özgür, M.; Korkmaz, Ş. Detailed transmittance analysis of high-performance SnO₂-doped WO₃ thin films in UV-Vis region for electrochromic devices. *J. Mat. Sci. Mat. Electron.* **2020**, *27*, 19074–19084. [[CrossRef](#)]
67. Yoneyama, H.; Haga, S.; Yamanaka, S. Photocatalytic activities of microcrystalline titania incorporated in sheet silicates of clay. *J. Phys. Chem.* **1989**, *93*, 4833–4837. [[CrossRef](#)]
68. Kabir, I.I.; Sheppard, L.R.; Shahmiri, R.; Liu, R.; Le, A.; Lu, X.; Hanaor, D.; Chen, W.F.; Koshy, P.; Sorrell, C.C. Correction to: Contamination of TiO₂ thin films spin coated on rutile and soda-lime-silica substrates. *J. Mat. Sci.* **2021**, *56*, 17874–17875. [[CrossRef](#)]
69. Zhao, J.; Cao, J.; Zhao, Y.; Zhang, T.; Zheng, D.; Li, C. Catalytic ozonation treatment of papermaking wastewater by Ag-doped NiFe₂O₄: Performance and mechanism. *J. Environ. Sci.* **2020**, *97*, 75–84. [[CrossRef](#)]

70. Xu, B.; Zhou, J.L.; Altaee, A.; Ahmed, M.B.; Johir, M.A.H.; Ren, J.; Li, X. Improved photocatalysis of perfluorooctanoic acid in water and wastewater by Ga₂O₃/UV system assisted by peroxymonosulfate. *Chemosphere* **2020**, *239*, 124722. [[CrossRef](#)]
71. Wang, L.; Zhang, Q.; Chen, B.; Bu, Y.; Chen, Y.; Ma, J.; Rosario-Ortiz, F.L. Photolysis and photocatalysis of haloacetic acids in water: A review of kinetics, influencing factors, products, pathways, and mechanisms. *J. Hazard. Mater.* **2020**, *391*, 122143. [[CrossRef](#)]
72. Tan, C.; Wu, H.; He, H.; Lu, X.; Gao, H.; Deng, J.; Chu, W. Anti-inflammatory drugs degradation during LED-UV365 photolysis of free chlorine: Roles of reactive oxidative species and formation of disinfection by-products. *Water Res.* **2020**, *185*, 116252. [[CrossRef](#)]
73. Park, K.Y.; Yu, Y.J.; Yun, S.J.; Kweon, J.H. Natural organic matter removal from algal-rich water and disinfection by-products formation potential reduction by powdered activated carbon adsorption. *J. Environ. Manag.* **2019**, *235*, 310–318. [[CrossRef](#)]
74. Majumder, A.; Gupta, B.; Gupta, A.K. Pharmaceutically active compounds in aqueous environment: A status, toxicity and insights of remediation. *Environ. Res.* **2019**, *176*, 108542. [[CrossRef](#)]
75. Sorlini, S. Natural Organic Matter: Characterization and Removal by AOPs to Assist Drinking Water Facilities. In *Applications of Advanced Oxidation Processes (AOPs) in Drinking Water Treatment*; Gil, A., Galeano, L.A., Vicente, M.A., Eds.; Springer: Cham, Switzerland, 2017; pp. 53–68.
76. Ghosh, D.; Mondal, S.; Ramakrishna, K. Pharmacobotanical, physicochemical and phytochemical characterisation of a rare salt-secreting mangrove *Aegialitis rotundifolia* Roxb., (Plumbaginaceae) leaves: A comprehensive pharmacognostical study. *South Afr. J. Bot.* **2017**, *113*, 212–229. [[CrossRef](#)]
77. Ganiyu, S.O.; Oturan, N.; Raffy, S.; Cretin, M.; Causserand, C.; Oturan, M.A. Efficiency of plasma elaborated sub-stoichiometric titanium oxide (Ti₄O₇) ceramic electrode for advanced electrochemical degradation of paracetamol in different electrolyte media. *Sep. Purif. Technol.* **2019**, *208*, 142–152. [[CrossRef](#)]
78. Zur, J.; Pinski, A.; Marchlewicz, A.; Hupert-Kocurek, K.; Wojcieszynska, D.; Guzik, U. Organic micropollutants paracetamol and ibuprofen-toxicity, biodegradation, and genetic background of their utilization by bacteria. *Environ. Sci. Pollut. Res.* **2018**, *25*, 21498–21524. [[CrossRef](#)]
79. Lopez Zavala, M.A.; Jaber Lara, C.R. Degradation of Paracetamol and Its Oxidation Products in Surface Water by Electrochemical Oxidation. *Environ. Eng. Sci.* **2018**, *35*, 1248–1254. [[CrossRef](#)]
80. Villota, N.; Lomas, J.M.; Camarero, L.M. Study of the paracetamol degradation pathway that generates color and turbidity in oxidized wastewaters by photo-Fenton technology. *J. Photochem. Photobiol. A Chem.* **2016**, *329*, 113–119. [[CrossRef](#)]
81. Neamtu, M.; Bobu, M.; Ketttrup, A.; Siminiceanu, I. Ozone photolysis of paracetamol in aqueous solution. *J. Environ. Sci. Health A Tox. Hazard. Subst. Environ. Eng.* **2013**, *48*, 1264–1271. [[CrossRef](#)]
82. Costamagna, P.; Delucchi, M.; Busca, G.; Giordano, A. System for ammonia removal from anaerobic digestion and associated ammonium sulfate production: Simulation and design considerations. *Proc. Safet. Environ. Protect.* **2020**, *144*, 133–142. [[CrossRef](#)]
83. Liu, F.; Sun, L.; Wan, J.; Tang, A.; Deng, M.; Wu, R. Organic matter and ammonia removal by a novel integrated process of constructed wetland and microbial fuel cells. *RSC Adv.* **2019**, *9*, 5384–5393. [[CrossRef](#)]
84. Kang, W.; Chen, S.; Yu, H.; Xu, T.; Wu, S.; Wang, X.; Lu, N.; Quan, X.; Liang, H. Photocatalytic ozonation of organic pollutants in wastewater using a flowing through reactor. *J. Hazard. Mater.* **2021**, *405*, 124277. [[CrossRef](#)]
85. Chen, X.; Zhan, S.; Chen, D.; He, C.; Tian, S.; Xiong, Y. Grey Fe-CeO₂-σ for boosting photocatalytic ozonation of refractory pollutants: Roles of surface and bulk oxygen vacancies. *Appl. Catal. B Environ.* **2021**, *286*, 119928. [[CrossRef](#)]
86. Asgari, E.; Sheikhmohammadi, A.; Nourmoradi, H.; Nazari, S.; Aghanaghad, M. Degradation of ciprofloxacin by photocatalytic ozonation process under irradiation with UVA: Comparative study, performance and mechanism. *Process Saf. Environ. Prot.* **2021**, *147*, 356–366. [[CrossRef](#)]
87. Zhou, Y.; Yang, D.; Lu, C.; Dai, S.; Li, J.; Guan, W.; Li, D. Enhanced photocatalytic ozonation of 2,4-dichlorophenoxyacetic acid using P25/g-C₃N₄ composite under visible light irradiation. *Desalination Water Treat.* **2020**, *208*, 377–385. [[CrossRef](#)]
88. Orge, C.A.; Sampaio, M.J.; Faria, J.L.; Pereira, M.F.R.; Silva, C.G. Efficiency and stability of metal-free carbon nitride in the photocatalytic ozonation of oxamic acid under visible light. *J. Environ. Chem. Eng.* **2020**, *8*, 104172. [[CrossRef](#)]
89. Bahadori, E.; Conte, F.; Tripodi, A.; Ramis, G.; Rossetti, I. Photocatalytic Selective Oxidation of Ammonia in a Semi-Batch Reactor: Unravelling the Effect of Reaction Conditions and Metal Co-Catalysts. *Catalysts* **2021**, *11*, 209. [[CrossRef](#)]
90. Joudi, F.; Naceur, J.B.; Ouertani, R.; Chtourou, R. A novel strategy to produce compact and adherent thin films of SnO₂/TiO₂ composites suitable for water splitting and pollutant degradation. *J. Mater. Sci. Mat. Electron.* **2018**, *30*, 167–179. [[CrossRef](#)]
91. Jiang, D.; Otitoju, T.A.; Ouyang, Y.; Shoparwe, N.F.; Wang, S.; Zhang, A.; Li, S. A Review on Metal Ions Modified TiO₂ for Photocatalytic Degradation of Organic Pollutants. *Catalysts* **2021**, *11*, 1039. [[CrossRef](#)]
92. Li, Y.; Li, W.; Liu, F.; Li, M.; Qi, X.; Xue, M.; Wang, Y.; Han, F. Construction of CeO₂/TiO₂ heterojunctions immobilized on activated carbon fiber and its synergetic effect between adsorption and photodegradation for toluene removal. *J. Nanopart. Res.* **2020**, *22*, 122. [[CrossRef](#)]